Cell Reports

Article

MacroH2As regulate enhancer-promoter contacts affecting enhancer activity and sensitivity to inflammatory cytokines

Graphical abstract

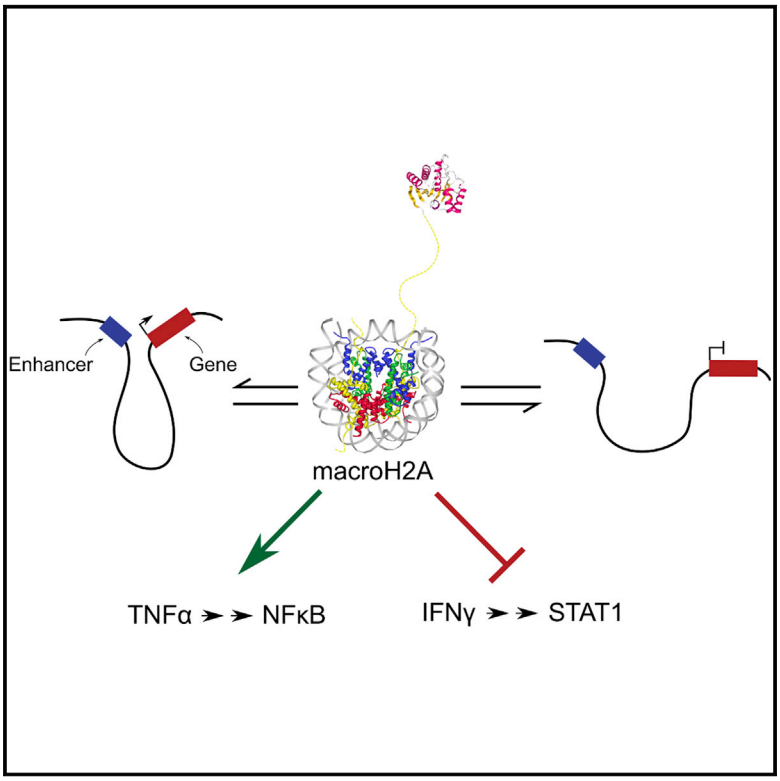

Authors

David Corujo, Roberto Malinverni, Juan Carrillo-Reixach, ..., Josep Manyé, Carolina Armengol, Marcus Buschbeck

Correspondence

carmengol@igtp.cat (C.A.), mbuschbeck@carrerasresearch.org (M.B.)

In brief

Corujo et al. show that the histone variants macroH2A1.2 and macroH2A2 regulate the response of cancer cells to inflammatory cytokines on the level of chromatin structure. MacroH2A-dependent changes in enhancer-promoter contacts are associated with increased sensitivity to tumor necrosis factor alpha and reduced sensitivity to interferon gamma.

Highlights

- MacroH2As facilitate the response of cancer cells to TNF-α-NF-κB but repress IFNγ-STAT1
- Changes in promoter-enhancer contacts co-occur or precede changes in enhancer activity
- MacroH2A2 is a more potent repressor of inflammatory response genes than macroH2A1.2

Corujo et al., 2022, Cell Reports *39*, 110988
June 21, 2022
https://doi.org/10.1016/j.celrep.2022.110988

CellPress

Cell Reports

CellPress
OPEN ACCESS

Article

MacroH2As regulate enhancer-promoter contacts affecting enhancer activity and sensitivity to inflammatory cytokines

David Corujo,[1,2] Roberto Malinverni,[1] Juan Carrillo-Reixach,[2,3] Oliver Meers,[1,4] Arce Garcia-Jaraquemada,[5] Marguerite-Marie Le Pannérer,[1,6] Vanesa Valero,[1] Ainhoa Pérez,[1] Álvaro Del Río-Álvarez,[2,3] Laura Royo,[2,3] Beatriz Pérez-González,[7] Helena Raurell,[7] Rafael D. Acemel,[8] José M. Santos-Pereira,[8] Marta Garrido-Pontnou,[9] José Luis Gómez-Skarmeta,[8] Lorenzo Pasquali,[7] Josep Manyé,[5,10] Carolina Armengol,[2,3,10,*] and Marcus Buschbeck[1,2,11,*]

[1]Cancer and Leukaemia Epigenetics and Biology Program, Josep Carreras Leukaemia Research Institute (IJC), Campus ICO-GTP-UAB, Badalona, Barcelona 08916, Spain
[2]Program for Predictive and Personalized Medicine of Cancer, Germans Trias i Pujol Research Institute (PMPPC-IGTP), Badalona, Barcelona 08916, Spain
[3]Childhood Liver Oncology Group, Germans Trias i Pujol Research Institute (IGTP), Badalona, Barcelona 08916, Spain
[4]Doctoral Programme in Biomedicine, Universitat de Barcelona, Facultat de Farmàcia i Ciències de l'Alimentació, Barcelona 08028, Spain
[5]IBD Research Group, Germans Trias i Pujol Research Institute (IGTP), Badalona, Barcelona 08916, Spain
[6]PhD Programme in Biomedicine, Universitat Pompeu Fabra, Barcelona 08003, Spain
[7]Department of Medicine and Life Sciences, Universitat Pompeu Fabra, Barcelona 08003, Spain
[8]Centro Andaluz de Biología del Desarrollo (CABD), CSIC-Universidad Pablo de Olavide-Junta de Andalucía, Sevilla 41013, Spain
[9]Pathology Department, Hospital Vall d'Hebron, Barcelona 08035, Spain
[10]Liver and Digestive Diseases Networking Biomedical Research Centre (CIBEREHD), Madrid 28029, Spain
[11]Lead contact
*Correspondence: carmengol@igtp.cat (C.A.), mbuschbeck@carrerasresearch.org (M.B.)
https://doi.org/10.1016/j.celrep.2022.110988

SUMMARY

MacroH2A histone variants have a function in gene regulation that is poorly understood at the molecular level. We report that macroH2A1.2 and macroH2A2 modulate the transcriptional ground state of cancer cells and how they respond to inflammatory cytokines. Removal of macroH2A1.2 and macroH2A2 in hepatoblastoma cells affects the contact frequency of promoters and distal enhancers coinciding with changes in enhancer activity or preceding them in response to the cytokine tumor necrosis factor alpha. Although macroH2As regulate genes in both directions, they globally facilitate the nuclear factor κB (NF-κB)-mediated response. In contrast, macroH2As suppress the response to the pro-inflammatory cytokine interferon gamma. MacroH2A2 has a stronger contribution to gene repression than macroH2A1.2. Taken together, our results suggest that macroH2As have a role in regulating the response of cancer cells to inflammatory signals on the level of chromatin structure. This is likely relevant for the interaction of cancer cells with immune cells of their microenvironment.

INTRODUCTION

Histone variants can replace replication-coupled histones in the nucleosome and endow chromatin regions with specific biochemical and biophysical characteristics (Martire and Banaszynski, 2020). Compared with replication-coupled histones, histone variants differ in sequence, expression timing, and mRNA processing (Buschbeck and Hake, 2017). Some of the most substantial sequence changes are found in three histone H2A variants known as macroH2As that share a peculiar tripartite structure consisting of the histone fold, a linker, and a macrodomain (Chakravarthy et al., 2005; Timinszky et al., 2009). Through alternative splicing, the MACROH2A1 gene (previously *H2AFY*) gives rise to the isoforms macroH2A1.1 and macroH2A1.2, while MACROH2A2 (previously H2AFY2) encodes macroH2A2 (Posavec et al., 2013). A large number of loss-of-function studies suggest that macroH2A proteins promote and stabilize differentiated cell states (Buschbeck and Hake, 2017). MacroH2A histone variants promote the differentiation of stem cells (Barrero et al., 2013a; Creppe et al., 2012) and inhibit the induction of pluripotency by nuclear transfer or by transduction of Yamanaka factors (Barrero et al., 2013b; Gaspar-Maia et al., 2013; Pasque et al., 2011). In cancer, the role of macroH2As is context- and isoform dependent (Ghiraldini et al., 2021). Reported observations include a tumor-suppressive function of macroH2A2 in melanoma (Kapoor et al., 2010) and an association of macroH2A1.1 with poor survival in triple-negative breast cancer (Lavigne et al., 2014).

The molecular basis for how macroH2A histone variants mediate these physiological and pathophysiological functions is not known. The field generally assumes that it is mediated through an influence on gene regulation. However, how macroH2A proteins impact on gene regulation is not understood. So far, we know that the presence of macroH2A on transcribed regions is associated with a repressed state (Gamble et al., 2010). This is explained by the fact that reincorporation of macroH2A relative to replication-coupled H2A is disfavored after passing of the polymerase complex in transcribed regions (Sun et al., 2018). On inactive genes, the presence of macroH2A provides a layer of repression in addition to histone deacetylation and DNA methylation (Hernández-Muñoz et al., 2005). However, deletion of macroH2As affects gene expression in both directions (Chen et al., 2014; Hurtado-Bagès et al., 2020), suggesting that the role of macroH2As is more complex than those of purely repressive chromatin components. In addition, macroH2A was found to be required for the proper induction of gene expression in response to different signals (Creppe et al., 2012; Dell'Orso et al., 2016; Ouararhni et al., 2006). One of the best-studied examples is the macroH2A1.1-dependent response of fibroblasts to a cocktail of cytokines secreted by senescent cells, which is essential for the propagation of the paracrine signal (Chen et al., 2015). Moreover, macroH2As have an important role in nuclear organization and are required for maintaining the characteristic three-dimensional architecture of heterochromatin (Douet et al., 2017), a function that can be mediated by the linker (Kozlowski et al., 2018). At present, it is not clear how the function in chromatin architecture ties in with transcriptional regulation.

To gain a better understanding of how macroH2A affects gene regulation in cancer, we have studied the transcriptional response to signals from innate immune cells. We have taken two different approaches. To study the response to a specific signal, we have chosen tumor necrosis factor alpha (TNF-α), which is one of the major pro-inflammatory cytokines involved in the innate immune response (Zelová and Hošek, 2013). Activated macrophages are the primary source of TNF-α, but other cells of the immune system can also secrete it. The role of TNF-α in cancer is complex. On one hand, TNF-α is an important effector of cytotoxic T cells and natural killer cells, but on the other, it can favor tumor growth and immune evasion (Balkwill, 2009). Signal transduction after TNF-α is mainly mediated by the canonical pathway involving the IKK complex and nuclear factor κB (NF-κB) transcription factors (Taniguchi and Karin, 2018). The NF-κB family is composed of 5 DNA-binding proteins that include RelA and RelB and that can form different homo- and heterodimeric transcription factors (Perkins, 2012). To study the impact of macroH2A on the inflammatory response in a more complex and natural environment, we have studied cells grown as xenografts in mice possessing intact innate immunity and analyzed previously generated datasets on primary patient samples.

Here, we describe how the levels of macroH2As modulate the ground state of transcription in a way that determines the quality of the response to inflammatory signals. Specifically, we present results showing that macroH2A1.2 and macroH2A2 affect the transcriptional responses to TNF-α and interferons in a complex and, to some extent, opposing manner. For TNF-α-response genes, we describe how macroH2A sensitivity is associated with differences in chromatin architecture and enhancer activity.

RESULTS

Loss of macroH2A1.2 and macroH2A2 globally modulates the transcriptional ground state

The loss of macroH2A histone variants has drastic consequences for nuclear organization and global three-dimensional (3D) heterochromatin architecture (Douet et al., 2017). To gain a better understanding of whether these changes are associated with changes in gene regulation, we have decided to study the loss of function of macroH2A on the transcriptional ground state and the response to innate immune signals. Specifically, we have used the hepatoblastoma-derived cell line HepG2 (López-Terrada et al., 2009) that expresses macroH2A1.2 and macroH2A2 but not macroH2A1.1 (Figure 1A). Short hairpin RNA (shRNA)-mediated knockdown allowed us to efficiently deplete both macroH2A proteins without notable compensation by macroH2A1.1 (Figure 1A). We reduced the serum concentration from the cell culture media to minimize the effect of stimuli coming from the complex composition of fetal bovine serum and analyzed the transcriptome in control and macroH2A-deficient HepG2 cells treated or not with TNF-α. Principal-component analysis confirmed the similarity of biological replicates and that both depletion of macroH2A and TNFα treatment affected the transcriptome (Figure 1B). Focusing first on the untreated condition, we found that a substantial number of genes were differentially expressed when comparing macroH2A-depleted cells with their controls (Figure 1C). The numbers of those up- and downregulated as well as their effect sizes were in a similar range. Top-enriched Gene Ontologies of upregulated genes were related to cell motility, metabolism, and the inflammatory response, while those of downregulated genes were related to morphogenesis, development, and adhesion (Figures 1D and 1E). Pathway analysis indicated downregulation of the PI3K pathway and upregulation of several pathways including WNT and JAK-STAT (Figure 1F). We observed similar macroH2A-dependent differences in gene expression when comparing macroH2A-depleted and control cells treated with TNF-α (Figures S1A–S1C). 60% of upregulated and 53% of downregulated genes overlapped in untreated and TNFα-treated cells, while the others were only differentially expressed in one of the two conditions (Figure S1D). In conclusion, the stable depletion of macroH2A1.2 and macroH2A2 in hepatoblastoma cells changes their transcriptional ground state.

Lack of macroH2A affects the transcriptional response to TNF-α

As expected, TNF-α prominently induced genes representing the inflammatory response, while repressed genes were related to metabolic pathways (Figures 2A and S2A–S2C). 663 (43.7%) of the total of 1,448 TNF-α-induced genes were further differentially expressed in macroH2A-depleted cells (Figure 2B). This proportion was significantly higher than for TNF-α-insensitive genes, defined as those that were readily detected but neither repressed nor induced by TNF-α treatment. 462 of these 633 genes were significantly less expressed in macroH2A-deficient

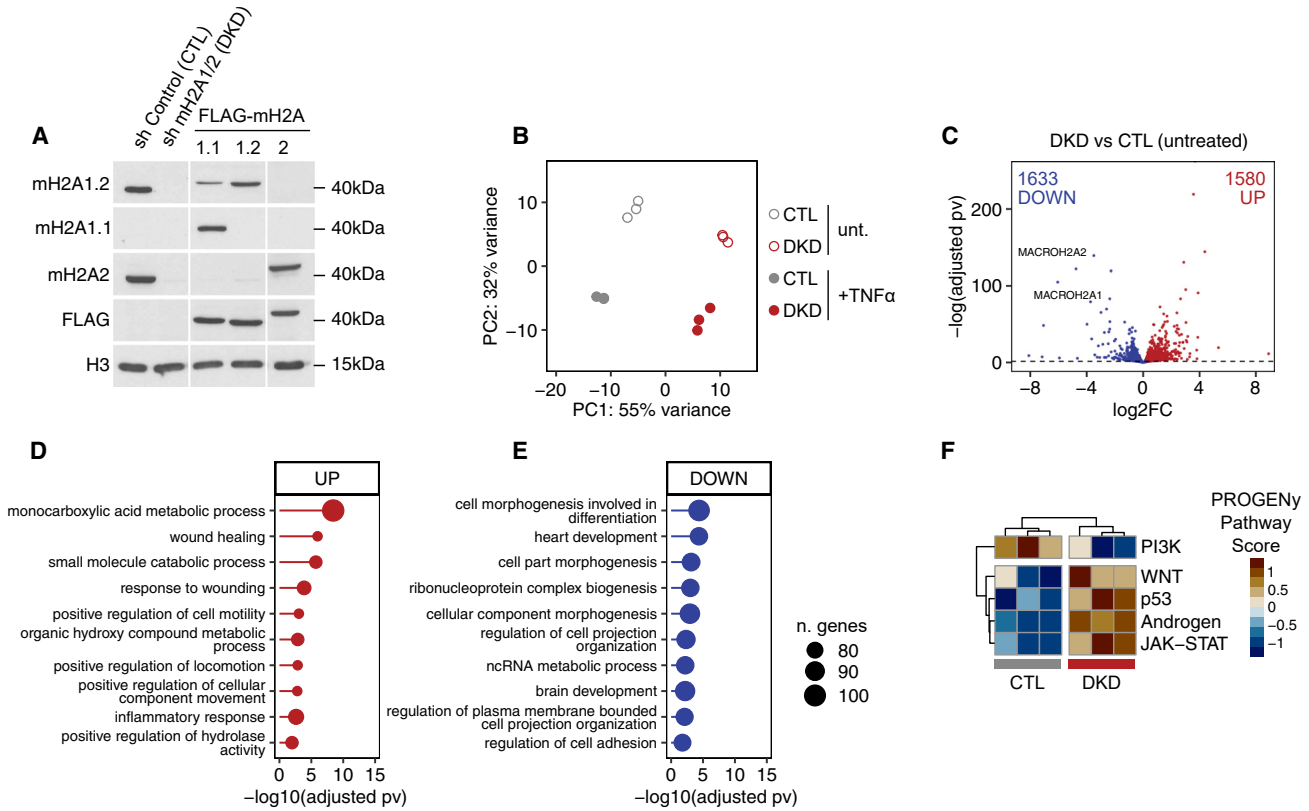

Figure 1. Loss of macroH2A modulates the transcriptional ground state of HepG2 cells

(A) Total cell extracts from double-knockdown (DKD) HepG2 cells stably transduced with shRNAs for macroH2A1 and macroH2A2 and control (CTL) cells were analyzed by immunoblotting using the indicated antibodies. Polyclonal DKD cells stably expressing equal amounts of FLAG-tagged macroH2A proteins were used as reference. All samples were detected on the same blotted membrane (per antibody), and white spaces indicate a separation where lanes of the blot have been re-arranged. The antibody used for macroH2A1.2 also detects macroH2A1.1, but as it is not expressed, the signal can be interpreted as macroH2A1.2.

(B) Principal-component (PC) plot of RNA sequencing (RNA-seq) samples from CTL and DKD cells treated or not with TNF-α at 20 ng/mL for 24 h. Three different replicates were seeded and treated on different days.

(C) Volcano plot of differentially expressed genes between DKD and CTL in untreated conditions plotted as log2 fold change (log2FC; Benjamini-Hochberg adjusted p value < 0.05).

(D) Top enriched Gene Ontologies in upregulated genes.

(E) Top enriched Gene Ontologies in downregulated genes.

(F) Inferred pathway activity using PROGENy.

cells (Figure 2C). A smaller proportion of TNF-α-induced genes (171 of 633) were further upregulated by loss of macroH2A. Using independent samples and semiquantitative PCR, we have confirmed the bidirectional influence of macroH2A depletion on a panel of TNF-α-induced genes (Figures 2D and 2E). Many of these genes were also differentially expressed in untreated conditions. Next, we analyzed the same panel of genes in a rescue setting in which we individually expressed exogenous macroH2A1.2 and macroH2A2 in macroH2A-depleted cells. From the immunoblot, we estimated that the achieved levels were close to the endogenous levels of macroH2A1.2 and macroH2A2 in parental HepG2 cells (Figure 1A). Interestingly, these levels of the individual macroH2A proteins were sufficient to partially rescue a subset of upregulated, but not downregulated, genes (Figures 2F, S3A, and S3B). In this, macroH2A2 was more potent than macroH2A1.2. In line with this observation, the individual knockdown of macroH2A2 upregulated five out of five tested upregulated genes, while the individual knockdown of macroH2A1.2 only affected one (Figures S3C and S3D). In contrast to the double knockdown, the individual knockdowns did not downregulate any of the 5 tested genes and in some cases even caused the opposite effect (Figure S3D).

Taken together, here we identify an enrichment between TNF-α- and macroH2A-regulated genes. The influence of macroH2As is bidirectional and requires the loss of both macroH2A1.2 and macroH2A2.

MacroH2A affects the activity and TNF-α sensitivity of some enhancers

To get a better understanding of how macroH2A affects gene regulation on the molecular level, we took a closer look at the extended genomic loci and in particular enhancers of three genes that were sensitive to both macroH2A depletion and TNF-α treatment. These included *DKK1*, whose expression

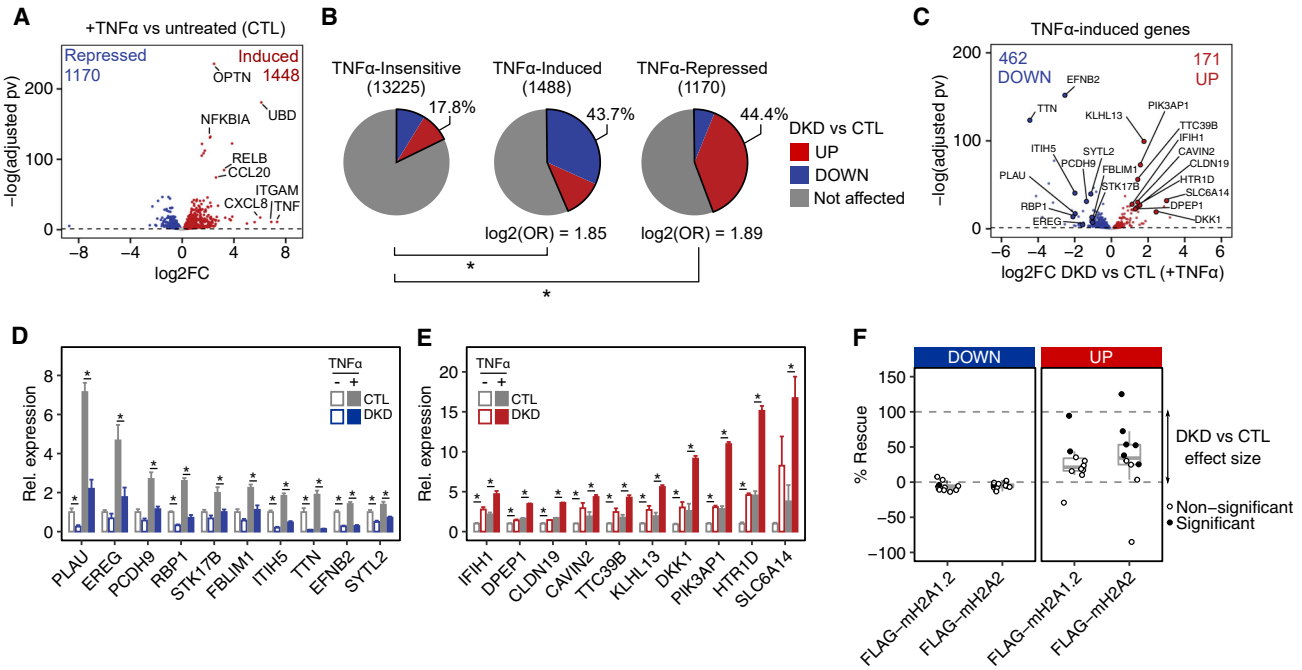

Figure 2. An enrichment between TNF-α- and macroH2A-regulated genes

(A) Volcano plot of the log2FC of gene expression comparing TNF-α-treated CTL cells with untreated CTL cells. All genes with an adjusted p value <0.05 were considered to be differentially expressed.

(B) Pie charts showing the enrichment of macroH2A-regulated genes among TNF-α-induced and -repressed genes relative to TNF-α-insensitive genes (detected at the same levels in treated and untreated conditions). A Fisher's exact test on a 2 × 2 contingency table has been used to make the indicated comparisons (*adjusted p value < 0.05; log2(OR), log2 odds ratio).

(C) Volcano plot of the log2FC of 633 macroH2A-sensitive, TNF-α-induced genes comparing CTL and DKD in TNF-α-treated conditions. The number of induced and repressed genes is indicated.

(D) Relative expression of a panel of TNF-α-induced genes downregulated in DKD cells compared with CTL cells assayed by qRT-PCR. TNF-α treatment was 20 ng/mL for 24 h (n = 3 biological replicates). A two-tailed Student's t test was used to make the indicated pairwise comparison. *p < 0.05.

(E) Same as in (E) for TNF-α-induced genes upregulated in DKD cells compared with CTL cells.

(F) FLAG-tagged macroH2A1.2 and macroH2A2 were individually and exogenously expressed in DKD cells. The resulting protein levels are shown in Figure 1A. The effect on the mRNA levels of 20 macroH2A and TNF-regulated genes (gene panels from D and E) was plotted for each gene relative to the difference between DKD and CTL (set to 100%). Significant rescues are indicated by dark bullets (p < 0.05, two-tailed Student's t test, n = 3 biological replicates). The full data used to generate this summary are shown in Figures S3A and S3B.

See also Figures S1–S3.

was increased already by macroH2A depletion and further by TNF-α treatment in a dose- and IKK-dependent manner, leading to increased secretion of WNT-antagonistic DKK1 protein (Figures S4A–S4C). Using our previously generated chromatin immunoprecipitation sequencing (ChIP-seq) data (Douet et al., 2017) and a peak-calling algorithm optimized for broader regions, we found that both macroH2A1.2 and macroH2A2 are enriched around the *DKK1* gene and several 3′ prime regions (Figure 3A). This broad signal is typical for macroH2A histone variants and makes the functional interpretation of their genomic profile challenging (Douet et al., 2017; Gamble et al., 2010; Ratnakumar et al., 2012). Here, we have used *epic2* (Stovner and Sætrom, 2019), a peak caller particularly aimed at identifying broad enrichment regions in diffuse ChIP-seq signals, to define domains of significant macroH2A1.2 and macroH2A2 enrichment. To identify and visualize regulatory enhancers of the *DKK1* gene, we have used the ROADMAP chromatin state annotation for HepG2 (Roadmap Epigenomics Consortium et al., 2015), the histone H3 K27 acetylation profile it is based on, and the regulatory annotation of the latest version of the GeneHancer database (Fishilevich et al., 2017). Taken together, these datasets suggest that the *DKK1* gene is regulated by several 3′ enhancers, of which the strongest coincides with the *MBL2* gene located at a distance of 0.45 Mb. Knockdown of macroH2A increased the expression of *MBL2* in a similar manner as *DKK1* but did not affect the much closer 5′ gene *PRKG1* or its antisense transcript *PRKG1-AS* (Figure S4D). According to an available ENCODE dataset in HepG2 cells, the NF-κB transcription factor RELA has a single annotated binding site at the *DKK1* gene promoter. Next, we tested whether depletion of macroH2A would affect the level of H3K27ac on 3′ enhancers as a proxy for their activity. We found that several of the tested enhancers, including those around the *MBL2* gene, increased their basal activity and their sensitivity to TNF-α (Figure 3B). On a second upregulated gene, *PIK3AP1*, macroH2A depletion affected the basal activity of two out of three tested enhancers located at 3' (Figures 3C and 3D). *EREG* is another TNF-α response gene but downregulated in macroH2A-depleted cells. Two 3′

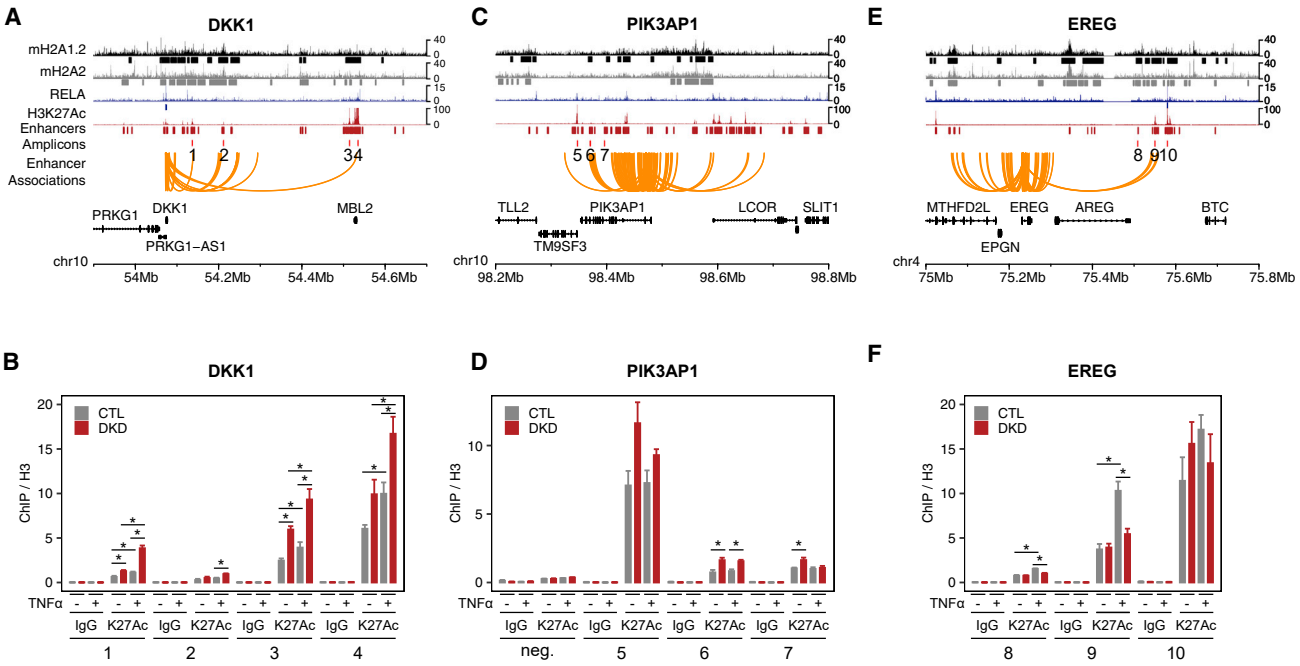

Figure 3. MacroH2A depletion affects the activity of enhancers of both up- and downregulated genes

(A) Genome browser view of the extended *DKK1* locus showing enrichment profiles for macroH2A1.2 macroH2A2, RELA, and H3K27ac in HepG2 cells. Peaks and regions of significant enrichment are indicated for macroH2A1.2, macroH2A2, and RELA below the enrichment profile. Enhancer regions are indicated using the annotation provided by the ROADMAP chromatin state of HepG2. Orange arches indicate functional gene-enhancer associations from a large compendium of cell types annotated in the GeneHancer database. The numbers indicate the position of amplicons used for ChIP-qPCR analysis in (B).

(B) ChIP-qPCR data for H3K27ac in the regions indicated in (A). Values have been normalized to H3 ChIP signal. Immunoglobulin G (IgG) is used as a negative CTL. Cells were cultured in the absence or presence of TNF-α at 20 ng/mL for 24 h (n = 4 biological replicates, *p < 0.05, two-tailed Student's t test on the indicated comparisons, K27Ac stands for H3K27Ac).

(C) Same as in (A) but for the extended locus for the upregulated gene *PIK3AP1*.

(D) Same as in (B) but for loci indicated in (C) and a negative CTL region (n = 3 biological replicates, *p < 0.05, two-tailed Student's t test on the indicated comparisons, K27Ac stands for H3K27Ac).

(E) Same as in (A) but for the downregulated gene *EREG*.

(F) Same as in (B) but for the loci indicated in (E) (n = 3 biological replicates, *p < 0.05, two-tailed Student's t test on the indicated comparisons, K27Ac stands for H3K27Ac).

See also Figure S4.

enhancers lost their sensitivity to TNF-α in macroH2A-depleted cells (Figures 3E and 3F). This was not the case for a third and neighboring enhancer that we tested and that happened to be bound by RELA in parental HepG2 cells. Importantly, the level of macroH2A1.2 and macroH2A2 enrichment at tested enhancers was low to intermediate and not affected by TNF-α treatment (Figures S4E and S4F).

Taken together, these results suggest that the absence and presence of macroH2A1.2 and macroH2A2 can affect both the activity of enhancers in their ground state as well as the sensitivity of enhancers to incoming inflammatory signals.

Changes in enhancer activity and sensitivity are associated with macroH2A-dependent changes in chromatin architecture

From our previous study, we know that loss of macroH2A has a drastic impact on large-scale chromatin organization in the nucleus. To get a better understanding of whether this also occurs in macroH2A-sensitive inflammatory response genes, we turned to chromosome-conformation-capture methods. Specifically, we have analyzed *DKK1-MBL2* and *EREG* as examples of genes that are up- or downregulated by macroH2A depletion after TNF-α treatment. We found that the *DKK1* gene was positioned at the 5′ end of a topologically associated domain (TAD) that spans a little more than 0.5 Mb and the MBL2 gene at the 3′ end (Figure 4A). This was indicated by contact probability maps from HiC data generated by ENCODE (Yardımcı et al., 2017) and our own HiChIP data generated with an antibody directed against H3 modified by trimethylation on lysine 4 (H3K4me3), a mark of active promoters. The H3K4me3 HiChIP data further showed that the *DKK1* promoter primarily established contacts with the downstream region inside the same TAD, including the regulatory distal enhancers located at the *MBL2* gene. Next, we used semiquantitative UMI-4C to probe for macroH2A-dependent changes in contact frequency of this regulatory region. In macroH2A-depleted cells, we observed increased contact with regions containing the DKK1 promoter and other macroH2A-sensitive enhancers 65 kb 3′ of DKK1 (Figure 4A, bottom panel). In control cells, these regions were enriched in macroH2A1.2 and macroH2A2. H3K4me3 HiChIP further showed

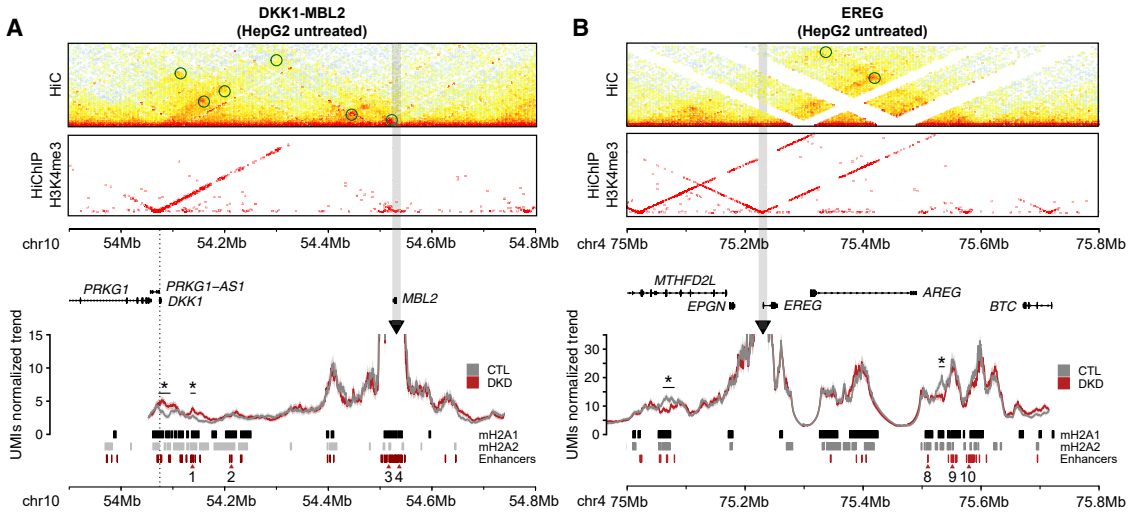

Figure 4. MacroH2A-regulated loci display changes in chromatin architecture

(A) Three-dimensional architecture of the *DKK1-MBL2* locus. The top panel shows the contact frequency maps of HepG2 HiC data generated by ENCODE. The middle panel shows the contact frequency map of the same region using H3K4me3 HiChIP data generated by us in untreated HepG2 cells. The bottom panel shows UMI-4C data that was used to quantify changes in contact frequency in untreated CTL and DKD HepG2 cell lines. The UMI-4C profile contains aggregated sequencing data from four biological replicates. The black arrow indicates the position of the viewpoint at the predicted regulatory region at the MBL2 gene locus. As in Figure 3A, enhancers and macroH2A-enriched regions are annotated. Red arrowheads indicate the regions analyzed by ChIP-qPCR in Figure 3B. The dotted line indicates the position of the *DKK1* promoter.

(B) Same as in (A) but for the extended *EREG* locus. The UMI-4C profile contains aggregated sequencing data from three biological replicates.

that the promoter of the downregulated gene *EREG* established contacts with regions both at 3′ and 5′ (Figure 4B). In the absence of macroH2A, two regions, one 5′ and one 3′, reduced contact frequency with the EREG promoter. Interestingly, both regions contained annotated regulatory enhancers and were enriched in macroH2A1.2 and macroH2A2.

Taken together, these results show that depletion of macroH2A1.2 and macroH2A results in changes in chromatin architecture and promoter-enhancer contacts. On the upregulated gene DKK1, increased expression and enhancer activity is associated with increased contacts. In the case of *EREG*, changes in chromatin architecture, specifically reduced contacts, preceded changes in gene expression and enhancer activity that were only observed after TNF-α treatment (Figure 3F).

MacroH2A has a complex function in inflammatory responses globally facilitating NFκB responses while inhibiting responses to interferon gamma (IFNγ)-STAT1

Our results so far have established that the presence and absence of macroH2A1.2 and macroH2A2 in HepG2 cells affects genes involved in the inflammatory response to TNF-α when treated in culture. To test whether macroH2A affects cells exposed to cytokines in a physiologic setting, we have decided to perform xenografts. From one of our previous studies, we know that HepG2 cells lacking macroH2A1.2 but retaining macroH2A2 are able to grow as xenografted tumors in immunosuppressed mice (Lo Re et al., 2017). Specifically, we injected macroH2A-deficient HepG2 cells and their control counterparts into partially immunosuppressed NOD.CB17-PRKDC^{SCID} mice (Figure 5A). These mice lack functional B and T cells but retain their innate immune system, making them a useful and frequently used model system for the study of cancer and autoimmune diseases (Bancroft and Kelly, 1994) https://www.jax.org/news-and-insights/2004/october/nod-cb17-prkdc-scid-j-strain-an-ideal-model-for-cancer-andautoimmune-disea#. While we did not observe any difference in growth or overall tissue composition (Figures S5A and S5B), we confirmed that the repression of MACROH2A1 and MACROH2A2 transcripts was stable and still prominent in xenografts after resection (Figure 5A). Next, we performed mRNA sequencing of five tumors of each experimental group. Principal-component analysis indicated that the overall expression pattern of xenografts was similar within the same group but greatly differed between groups (Figure S5C). Using an adjusted p value of 0.05 as cutoff, we identified 2,113 genes to be downregulated and 2,293 to be upregulated when comparing macroH2A-deficient xenografts with their control counterparts (Figure 5B). Both MACROH2A1 and MACROH2A2 were among the most downregulated genes, thus validating the performance of our mRNA sequencing. Enriched Gene Ontologies included ribosomal pathways in downregulated genes and catabolic processes in upregulated genes (Figure S5D). Gene set enrichment analysis indicated an enrichment of genes related with the inflammatory response (Figure 5C) among the upregulated genes. In addition, genes related to hypoxia were enriched among the upregulated genes (Figure S2E), which resonated previous findings relating macroH2A1 isoforms to redox metabolism in breast cancer cells (Dardenne et al., 2012). To gain a better understanding of the pathways mediating the observed transcriptional changes, we have used a method to infer transcription factor activity (Alvarez et al., 2016; Garcia-Alonso et al., 2019). Among the downregulated regulons in macroH2A-deficient xenografts was the NF-κB transcription factor RELB (Figure 5D), which is part of the canonical signaling pathway of TNF-α (Zelová and Hošek, 2013). This is in

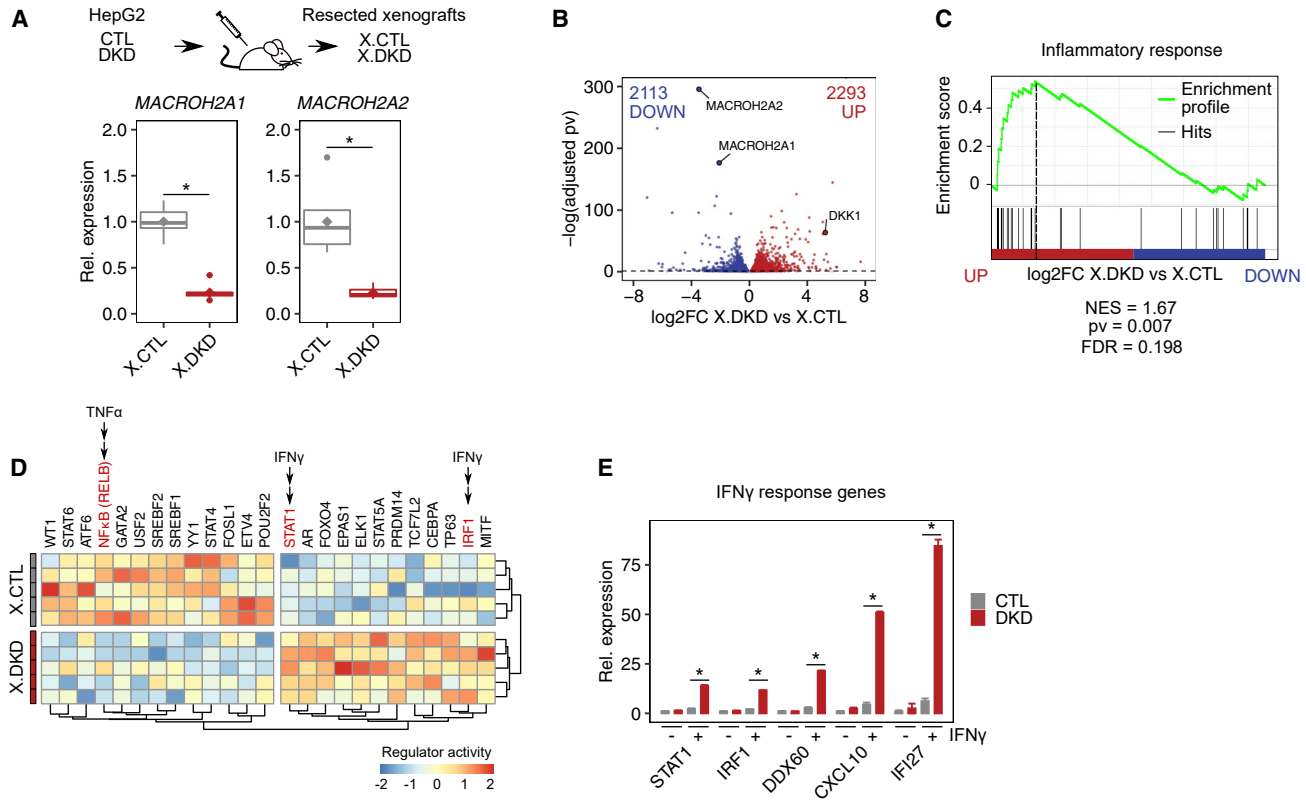

Figure 5. MacroH2A proteins affect the quality of the inflammatory response *in vivo*

(A) Relative expression of macroH2A1- and macroH2A2-encoding transcripts in resected xenografts of macroH2A-deficient HepG2 cells (X.DKD) and CTL cells (X.CTL) was assayed by qRT-PCR. Rhombi indicate the mean values and thick horizontal lines the median values per group (n = 10 tumors per condition, a two-tailed Student's t test was used to make the indicated pairwise comparison, *p < 0.05).

(B) Volcano plot of differentially expressed genes between X.DKD and X.CTL in untreated conditions plotted as log2FC (Benjamini-Hochberg adjusted p value < 0.05). The number of up- and downregulated genes are given.

(C) Gene set enrichment profile using all significantly differentially expressed genes ranked by their log2FC. The M5932 - HALLMARK_INFLAMMATORY_RESPONSE gene set from the Molecular Signatures Database is shown. NES, normalized enrichment score; FDR, false discover rate; pv, p value.

(D) Gene expression count matrices were used to infer changes in regulon activity using *VIPER* and the *DoRothEA* regulon sets. Mediators of IFNγ (STAT1 and IRF1) and TNF-α signaling (NF-κB) are indicated. Values in the heatmap are scaled by column.

(E) Expression of STAT1, IRF1, and three IFNγ response genes assayed by qRT-PCR in HepG2 CTL and DKD cultured in the absence or presence of IFNγ at 100 ng/mL for 48 h (n = 3 biological replicates, a two-tailed Student's t test was used to make the indicated pairwise comparison, *p < 0.05).

See also Figure S5 and Table S1.

line with our observation that loss of macroH2A led to a substantially larger number of TNF-α-induced genes being down- than upregulated (Figure 2B). Upregulated regulons included IFN regulatory factor 1 (IRF1) and STAT1, two well-known mediators of another type of pro-inflammatory signaling (Figure 5D). Specifically, IRF1 and STAT1 are the main transcriptional mediators of IFNs, which are central cytokines of the innate immune response (Feng et al., 2021). To test an influence of macroH2A on IFN signaling, we turned again to cell culture and analyzed known IFNγ response genes in macroH2A-deficient HepG2 and control cells. The expression of the transcription factors *STAT1* and *IRF1* as well as the IFNγ-response genes *CXCL10*, *DDX60*, and *IFI27* was strongly increased in cells lacking macroH2A upon treatment with IFNγ (Figure 5E).

Taken together, the growth of macroH2A-deficient and control HepG2 cells as xenografts allowed us to investigate their response in a more natural environment of cytokines. The transcriptomic analysis points toward a complex role of macroH2A in inflammatory signaling. The net output of macroH2A's presence is, on one hand, the promotion of TNF-α-NF-κB signaling and, on the other, a suppression of IFNγ-STAT1 signaling.

MacroH2A1 expression levels are related to inflammatory transcription factor activity in hepatoblastoma tumor samples

The association of macroH2A variants with cancer is context- and isoform dependent. In cancers of the liver tissue, both cancer-promoting and -repressing functions have been attributed to macroH2A histone variants (Hsu et al., 2021). Hepatoblastoma is the most common type of pediatric liver cancer and usually develops in infants and young children during the first 3 years of life (Schnater et al., 2003). We have recently described a detailed

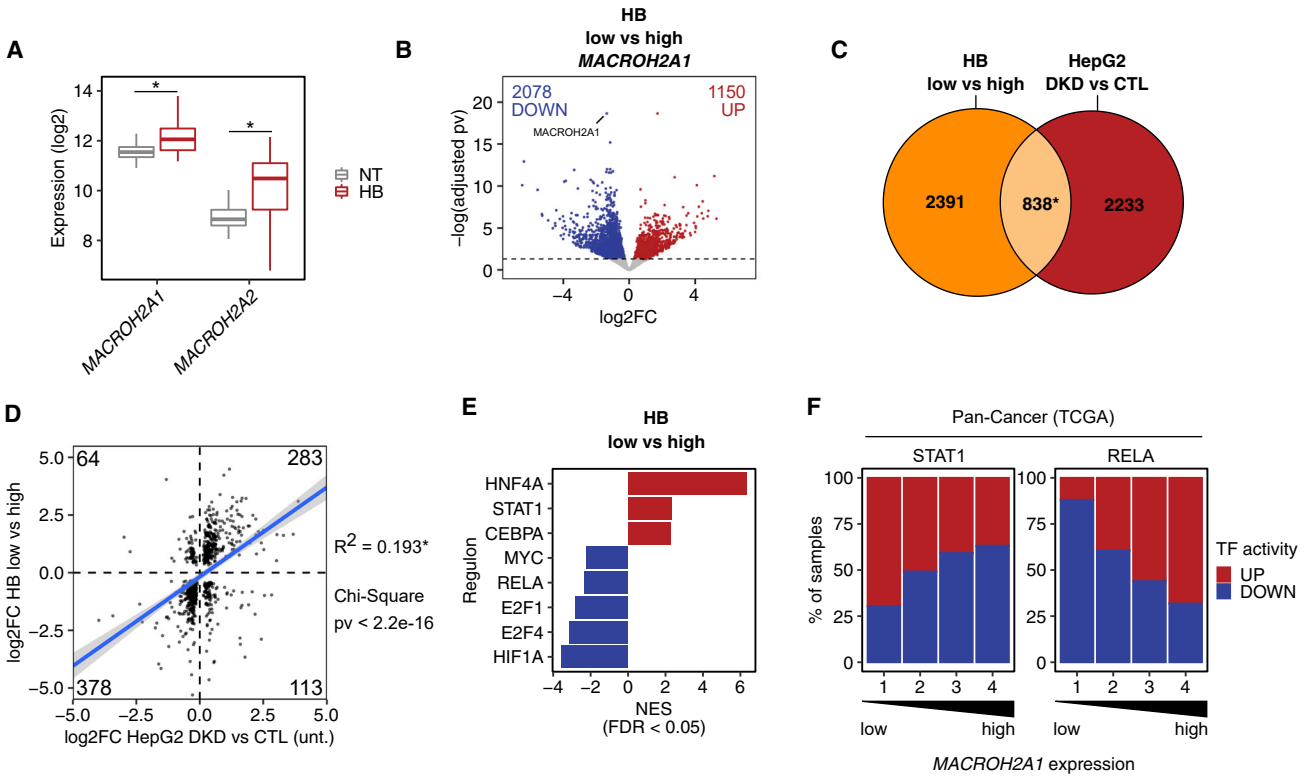

Figure 6. MacroH2A1 expression levels are related to inflammatory transcription factor activity in hepatoblastoma primary tumor samples

(A) Boxplot showing the log2 expression values of MACROH2A1 and MACROH2A2 for 32 hepatoblastoma (HB) tumor samples and matched non-tumor (NT) tissue samples. An unpaired t test with Welch correction was used to compare the two groups, *p < 0.05.

(B) Volcano plot of differentially expressed genes between the tercile of HB tumors with lowest and highest MACROH2A1 expression (log2FC; Benjamini-Hochberg adjusted p value < 0.05). For tercile separation, please see Figure S6A.

(C) Venn diagram showing the significant overlap of differentially expressed genes in low versus high MACROH2A1 and DKD versus CTL (both datasets have been reduced to the genes that have been detected in both experiments). A Fisher's exact test was used to evaluate the significance of the overlap, *p < 0.05.

(D) Scatterplot of log2FC values of the differentially expressed genes between low versus high MACROH2A1 and DKD versus CTL. The blue line represents the regression line obtained by fitting a linear model on the data points, and R^2 is the coefficient of determination of the resulting linear regression model ($p < 2.16 \times 10^{-16}$). A chi square test of independence has been performed on the categories defined by the four quadrants, and the p value is reported.

(E) Regulon activity as annotated in *DoRothEA* has been inferred with *VIPER*, and normalized enrichment scores (NESs) with a false discovery rate (FDR) < 0.05 are plotted.

(F) The samples from the TCGA Pan-Cancer cohort with up- or downregulated inferred activities of the transcription factors STAT1 (n = 1,000) and NF-κB (RELA; n = 256) by the *RABIT* algorithm were ranked in four quartiles according to their MACROH2A1 expression values. The proportion in percentage of samples with up- or downregulated activities for each transcription factor is plotted for each quartile.

See also Figure S6.

molecular characterization of one of the largest cohorts of patients with hepatoblastoma (HB) (Carrillo-Reixach et al., 2020). This analysis included the transcriptome-wide analysis of 32 paired tumor and adjacent normal liver tissues. While the data did not allow us to resolve differences between the two macroH2A1 splice isoforms, it showed that total levels of macroH2A1 and macroH2A2 transcripts were upregulated in tumor tissues compared with adjacent normal tissue and that MACROH2A1 was more prominently expressed than MACROH2A2 (Figure 6A). We have separated the tumor samples in low, medium, and high *MACROH2A1*-expressing tumors (Figure S6A). Comparison of low with high expressing tumors identified 3,229 differentially expressed genes (Figure 6B). A significant proportion of these genes (838) were overlapping with genes differentially expressed in macroH2A-depleted HepG2 compared with control cells (Figure 6C). The correlation between both datasets was positive, as the large majority were differentially expressed in a concordant manner (Figure 6D). However, this was not the case for MACROH2A2 (Figures S6B–S6E). Pathway analysis of the HB tumor samples indicated that low MACROH2A1 levels were associated with increased STAT1 signaling and reduced activity of the NF-κB transcription factor RELA (Figure 6E). Low MACROH2A2 levels were also associated with increased STAT1 signaling but, in contrast to MACROH2A1, also with higher levels of RELA activity (Figure S6F). To test whether this differential role of macroH2A could be more general and not restricted to HB, we turned to data of the Pan-Cancer cohort of The Cancer Genome Atlas (TCGA). We have divided all samples with an up- or downregulated inferred transcription factor activity for STAT1 and the NF-κB transcription factor RELA in 4

quartiles of macroH2A1 expression (Figures S6B and S6C). As shown in Figure 6F, high STAT1 activity was preferentially found in low *MACROH2A1*-expressing samples, while high NF-κB activity was associated with high MACROH2A1 levels. For MACROH2A2, we observed the same inverse correlation with STAT1 activity and, to a lesser extent, a positive correlation with NF-κB activity (Figure S6G).

In conclusion, the transcriptomic analyses of cell cultures and xenografts after macroH2A depletion and the comparison of high and low macroH2A-expressing HB samples suggest that macroH2A variants have a role in modulating the inflammatory response of liver cancer cells. Taken together, our results suggest that the presence of macroH2A facilitates NF-κB responses while inhibiting IFNγ-STAT1 responses. The similar association between transcription factor activity and macroH2A levels in the large Pan-Cancer cohort of TCGA suggests that this bidirectional function of macroH2A is more general.

DISCUSSION

Here, we provide evidence that macroH2A modulates the transcriptional response of cancer cells to inflammatory signaling on the level of chromatin. MacroH2A histone variants do so in an unprecedented manner, facilitating some responses while dampening others. This involves the regulation of enhancers and 3D chromatin architecture of sensitive loci. We will focus our discussion on two major points. First, we will discuss possible molecular mechanisms by which macroH2A could impact on enhancer elements. Second, we will discuss an emerging role of macroH2A in regulating autocrine and paracrine signaling and its relevance for cancer.

How macroH2A affects gene regulation is poorly understood. Here, we found that depletion of both macroH2A1.2 and macroH2A2 affected the transcriptional ground state of cancer cells involving both the up- and downregulation of a large number of genes. When focusing on inflammatory response genes defined by the upregulation after treatment with TNF-α, we found that macroH2A-regulated genes were strongly overrepresented. Interestingly, the regulation of these genes required the stable depletion of both macroH2A1.2 and macroH2A2, since neither depletion nor re-expression of macroH2A1.2 or macroH2A2 alone was sufficient to elicit or rescue, respectively, the full effect observed in the double knockdown cells. Interestingly, we found that upregulated genes were generally more sensitive to perturbations of individual macroH2As than downregulated genes, possibly suggesting that repression is more directly linked to the presence of macroH2A. The effect of perturbing macroH2A2 alone was greater than macroH2A1.2 alone. We have further studied the genomic loci of three macroH2A-regulated TNF-α response genes in greater detail. MacroH2A depletion led to changes in gene expression associated with changes in H3K27ac levels on distal enhancers. In several cases, these changes already occurred in the absence of TNF-α and were associated with changes in 3D chromatin architecture including enhancer-promoter contacts. In cases where changes in gene expression, enhancer activity measured by H3K27ac, and enhancer-promoter activity coincide, we are unable to distinguish cause and consequence. However, in the case of *EREG*, we observed a reduction of enhancer-promoter contacts that preceded changes in gene expression and enhancer activity after TNF-α treatment. Taken together, results are compatible with the hypothesis that the influence of macroH2A on enhancers is downstream of its influence on 3D chromatin architecture. Interestingly, identified sites of gained contacts in *DKK1-MBL2* locus as well as sites that lost contact in the *EREG* locus were enriched in macroH2A. In our future study, we will test whether this functional association exists genome wide.

Others have previously put forward the hypothesis that highly localized macroH2A-containing nucleosomes might affect the binding of transcription factors to their regulatory elements. In support of this hypothesis, macroH2A1.2-containing nucleosomes interfered with NF-κB binding *in vitro* (Angelov et al., 2003) and with ATF2 binding in B cells (Agelopoulos and Thanos, 2006), while in myogenic cells, macroH2A1.2 promoted the recruitment of Pbx1 to enhancers (Dell'Orso et al., 2016). In a more general manner, singular macroH2A-containing nucleosomes positioned on promoters were suggested to facilitate the binding of some transcription factors while repelling others, thereby contributing to transcriptional robustness (Lavigne et al., 2015). However, in most cell types, including the here-used HepG2 cells, macroH2A is widely distributed in the genome, and this distribution profile is not compatible with highly positioned nucleosomes on promoters or enhancers (Changolkar et al., 2010; Douet et al., 2017; Gamble et al., 2010; Ratnakumar et al., 2012). Attempts to quantify the distribution of macroH2A have estimated that up 30% of the genome contains some enrichment of macroH2A (Gamble et al., 2010), which needs to be put into context with the fact that, in most cell types, macroH2A1 levels make up 1% of the histone H2A pool (Buschbeck and Hake, 2017; Leroy et al., 2013). This means that most genomic regions scored as macroH2A bound by ChIP-seq or similar epigenomic methods are likely not saturated for macroH2A binding. A plausible interpretation of these observations is that the exact positioning of macroH2A proteins is less relevant for their function and that their presence in few nucleosomes possibly interspersed with nucleosomes containing other H2As might suffice for macroH2A to exert its molecular function. An important lesson comes from heterochromatin where intermediate levels of macroH2A enrichment are sufficient to mediate 3D compaction in the nuclear space and its association with the nuclear lamina (Douet et al., 2017). Future studies will be needed to resolve the causality of macroH2A-dependent alterations in 3D chromatin architecture and gene regulation.

In our study, we have focused on the response of HB cells to the acute inflammatory signal induced by the cytokine TNF-α. Although ablation of macroH2A led to the increased expression of some TNF-α response genes such as *DKK1* and *PIK3AP1*, globally, the effect was a dampening of the TNF-α response. Most interestingly, we found that macroH2A had the opposite role for the response to IFNγ mediated by JAK-STAT signaling, which is also observed in cancer-associated fibroblasts (Filipescu et al., 2022). IFNγ is a pleiotropic cytokine that can have cytotoxic effects on tumor cells and promote the recruitment and action of immune cells to target tumor cells but, at the same time, can induce proliferation of cancer cells and other pro-tumorigenic effects (Gocher et al., 2021). To our knowledge,

such a chromatin-regulated shift in the relative response to two major cytokines of the innate immunity has not been reported so far, and its physiological consequences remain elusive. Furthermore, it will be interesting to assess to what extent the role of macroH2A extends to other paracrine stimuli from the microenvironment and in particular immune cells.

Several lines of evidence indicate that macroH2A in cancer cells might also play a role in the opposite direction shaping the microenvironment through its impact on secretory pathways. In breast and prostate cancers, macroH2A inhibits genes encoding secreted factors promoting osteoclastogenesis (Kim et al., 2018a, 2018b). Inversely, others have reported a positive influence. In hepatocellular carcinoma cells, for instance, macroH2A depletion promotes the secretion of cytokines and chemokines affecting the activation state of exposed lymphocytes (Lo Re et al., 2020). This included an increased secretion of TNF-α, which, combined with our results, indicates that macroH2A can regulate cancer cells through autocrine loops. In human fibroblasts, macroH2A is required for the response to senescence-inducing factors and promoted the expression of genes encoding them, thereby propagating the signal in a paracrine manner (Chen et al., 2015). The here-identified macroH2A-repressed gene *DKK1* encodes a paracrine factor that is a well-described negative regulator of the WNT signaling pathway (Huang et al., 2018). The literature describes a number of cancer-promoting functions for *DKK1* that include a contribution to immune evasion of disseminated cancer cells (Malladi et al., 2016). Interestingly, a previous study has assigned opposing roles for macroH2A1 and *DKK1* in affecting colorectal cancer progression through senescence (De Barrios et al., 2017).

Taken together, a picture emerges placing macroH2A in a central role in intercellular communication by affecting, on one hand, the response to inflammatory signals and, on the other, the baseline and inducible expression of genes encoding autocrine and paracrine factors. Depending on the signal and its intracellular pathway, macroH2A can both enhance or suppress the intensity of the inflammatory response. This has implications for understanding the interaction of cancer cells with cells of their microenvironment and, in particular, immune cells. An inflammatory microenvironment has been recognized as a hallmark of cancer (Hanahan and Weinberg, 2011). Specifically, after failed elimination of a nascent tumor by immune cells, a switch in the quality of the immune reaction including changes in the polarization of tumor-associated macrophages can promote tumor progression and immune evasion (Galdiero et al., 2018). The evasion of the immune system is recognized as another hallmark of cancer (Hanahan and Weinberg, 2011). In the future, it will be exciting to further dissect how macroH2A-regulated paracrine signaling modulates the interaction of cancer cells with their microenvironment and to evaluate the relevance of this regulatory axis for immune therapy.

Limitations of the study

In this study, we have studied transcriptional changes after stable depletion of macroH2As in HepG2 cells upon TNF-α treatment for 24 h. These time frames limit our capability of distinguishing direct and indirect effects. The detailed characterization of enhancer activity and chromatin conformation has been performed on representative gene loci. The limited number of these examples limits our capacity to generalize our observation that macroH2A-dependent changes in 3D chromatin architecture co-occur or precede changes in enhancer activity. The combination of genome-wide approaches with faster perturbation methods will be needed to overcome these limitations in the future.

STAR★METHODS

Detailed methods are provided in the online version of this paper and include the following:

- KEY RESOURCES TABLE
- RESOURCE AVAILABILITY
  - Lead contact
  - Materials availability
  - Data and code availability
- EXPERIMENTAL MODEL AND SUBJECT DETAILS
  - Cell lines
  - Animals
- METHOD DETAILS
  - Cloning of plasmids
  - Cell lines, culture condition, gene transduction and treatments
  - Xenografts
  - Immunoblotting
  - RNA isolation and gene expression analysis by RT-qPCR
  - Transcriptomic analysis
  - Enrichment analysis of gene sets and gene ontologies
  - Inference of pathway and transcription factor activity from transcriptomic data
  - Chromatin immunoprecipitation
  - UMI-4C
  - HiChIP
  - Use of published datasets
- QUANTIFICATION AND STATISTICAL ANALYSIS

SUPPLEMENTAL INFORMATION

Supplemental information can be found online at https://doi.org/10.1016/j.celrep.2022.110988.

ACKNOWLEDGMENTS

We thank François Le Dily (CRG, Spain) for his help with sequencing the UMI4C samples, members of the M.B. lab for valuable discussion of the results, and the staff of IJC and IGTP core facilities for excellent support. Some of our results have been obtained using data generated by the TCGA Research Network (https://www.cancer.gov/tcga). This research project was supported by the national grants RTI2018-094005-B-I00 and BFU2015-66559-P from FEDER/Ministerio de Ciencia e Innovación - Agencia Estatal de Investigación (to M.B.); PI09/00751, PI10/02082, and PI13/02340 from the Instituto de Salud Carlos III (to C.A.); the MECD fellowship FPU14/06542 (to D.C.); AGAUR 2019 FI_B01024 and 2022 FI_B00528 fellowships (to J.C.-R. and A.D.R.-A., respectively); and predoctoral fellowships BES-2016-077251 (to M.-M.L.P.) and PRE2019-088529 (to O.M.). Research in the M.B. lab is further supported by the following grants: the Marie Skłodowska Curie Training network "INTERCEPT-MDS" H2020-MSCA-ITN-2020-953407 (to M.B.); MINECO-ISCIII PIE16/00011 (to M.B.); the Deutsche José Carreras

Leukämie Stiftung DJCLS 14R/2018 (to M.B.); AGAUR 2017-SGR-305 (to M.B.); and Fundació La Marató de TV3 257/C/2019 (to M.B.). C.A.'s research has received funding from the European Union's Horizon 2020 research and innovation program under grant agreement nos. 668596 (ChiLTERN) and 826121 (iPC) as well as from CIBERehd (CB06/04/0033) and AGAUR (2017-SGR-490). C.A. was supported by Ramón y Cajal (RYC-2010-07249) of the Ministry of Science and Innovation of Spain. Research at the IJC is supported by the "La Caixa" Foundation, the Fundació Internacional Josep Carreras, Celgene Spain, and the CERCA Programme/Generalitat de Catalunya.

AUTHOR CONTRIBUTIONS

Conceptualization, D.C. and M.B.; data curation, R.M. and J.C.-R.; formal analysis, R.M., D.C., A.D.R.-A., J.C.-R., and M.G.-P.; funding acquisition, C.A. and M.B.; investigation, D.C., V.V., A.P., A.G.-J., M.-M.L.P., L.R., H.R., and O.M.; methodology, B.P.-G., R.D.A., J.M.S.-P., J.L.G.-S., and L.P.; resources, C.A.; supervision, J.M., J.L.G.-S., C.A., L.P., and M.B.; writing – original draft, D.C. and M.B.; writing – review and editing, C.A.

DECLARATION OF INTERESTS

The authors declare no competing interests.

Received: October 19, 2021
Revised: April 4, 2022
Accepted: May 31, 2022
Published: June 21, 2022

REFERENCES

Abugessaisa, I., Noguchi, S., Hasegawa, A., Kondo, A., Kawaji, H., Carninci, P., and Kasukawa, T. (2019). refTSS: a reference data set for human and mouse transcription start sites. J. Mol. Biol. *431*, 2407–2422. https://doi.org/10.1016/j.jmb.2019.04.045.

Agelopoulos, M., and Thanos, D. (2006). Epigenetic determination of a cell-specific gene expression program by ATF-2 and the histone variant macroH2A. EMBO J. *25*, 4843–4853. https://doi.org/10.1038/sj.emboj.7601364.

Alvarez, M.J., Shen, Y., Giorgi, F.M., Lachmann, A., Ding, B.B., Hilda Ye, B., and Califano, A. (2016). Functional characterization of somatic mutations in cancer using network-based inference of protein activity. Nat. Genet. *48*, 838–847. https://doi.org/10.1038/ng.3593.

Angelov, D., Molla, A., Perche, P.Y., Khochbin, S., Côté, J., Hans, F., Co, J., Bouvet, P., Dimitrov, S., Merci, D.D., et al. (2003). The histone variant MacroH2A interferes with transcription factor binding and SWI/SNF nucleosome remodeling. Mol. Cell *11*, 1033–1041. https://doi.org/10.1016/s1097-2765(03)00100-x.

Balkwill, F. (2009). Tumour necrosis factor and cancer. Nat. Rev. Cancer *9*, 361–371. https://doi.org/10.1038/nrc2628.

Barrero, M.J., Sese, B., Martí, M., and Izpisua Belmonte, J.C. (2013a). Macro histone variants are critical for the differentiation of human pluripotent cells. J. Biol. Chem. *288*, 16110–16116. https://doi.org/10.1074/jbc.m113.466144.

Bancroft, Gregory, J, and Kelly, John, P. (1994). Macrophage Activation and Innate Resistance to Infection in SCID Mice. Immunobiology *191* (*4*), 424–431. https://doi.org/10.1016/S0171-2985(11)80448-1.

Barrero, M.J., Sese, B., Kuebler, B., Bilic, J., Boue, S., Martí, M., Martí, M., and Izpisua Belmonte, J.C. (2013b). Macrohistone variants preserve cell identity by preventing the gain of H3K4me2 during reprogramming to pluripotency. Cell Rep. *3*, 1005–1011. https://doi.org/10.1016/j.celrep.2013.02.029.

De Barrios, O., Győrffy, B., Fernández-Aceñero, M.J., Sánchez-Tilló, E., Sánchez-Moral, L., Siles, L., Esteve-Arenys, A., Roué, G., Casal, J.I., Darling, D.S., et al. (2017). ZEB1-induced tumourigenesis requires senescence inhibition via activation of DKK1/mutant p53/Mdm2/CtBP and repression of macroH2A1. Gut *66*, 666–682. https://doi.org/10.1136/gutjnl-2015-310838.

Buschbeck, M., and Hake, S.B. (2017). Variants of core histones and their roles in cell fate decisions, development and cancer. Nat. Rev. Mol. Cell Biol. *18*, 299–314. https://doi.org/10.1038/nrm.2016.166.

Buschbeck, M., Uribesalgo, I., Wibowo, I., Rué, P., Martin, D., Gutierrez, A., Morey, L., Guigó, R., López-Schier, H., and Di Croce, L. (2009). The histone variant macroH2A is an epigenetic regulator of key developmental genes. Nat. Struct. Mol. Biol. *16*, 1074–1079. https://doi.org/10.1038/nsmb.1665.

Cantariño, N., Fernández-Figueras, M.T., Valero, V., Musulén, E., Malinverni, R., Granada, I., Goldie, S.J., Martín-Caballero, J., Douet, J., Forcales, S.V., et al. (2016). A cellular model reflecting the phenotypic heterogeneity of mutant HRAS driven squamous cell carcinoma. Int. J. Cancer *139*, 1106–1116. https://doi.org/10.1002/ijc.30139.

Carrillo-Reixach, J., Torrens, L., Simon-Coma, M., Royo, L., Domingo-Sàbat, M., Abril-Fornaguera, J., Akers, N., Sala, M., Ragull, S., Arnal, M., et al. (2020). Epigenetic footprint enables molecular risk stratification of hepatoblastoma with clinical implications. J. Hepatol. *73*, 328–341. https://doi.org/10.1016/j.jhep.2020.03.025.

Chakravarthy, S., Gundimella, S.K.Y., Caron, C., Perche, P.-Y., Pehrson, J.R., Khochbin, S., and Luger, K. (2005). Structural characterization of the histone variant macroH2A. Mol. Cell Biol. *25*, 7616–7624. https://doi.org/10.1128/mcb.25.17.7616-7624.2005.

Changolkar, L.N., Singh, G., Cui, K., Berletch, J.B., Zhao, K., Disteche, C.M., and Pehrson, J.R. (2010). Genome-wide distribution of macroH2A1 histone variants in mouse liver chromatin. Mol. Cell Biol. *30*, 5473–5483. https://doi.org/10.1128/mcb.00518-10.

Chen, H., Ruiz, P.D., Novikov, L., Casill, A.D., Park, J.W., and Gamble, M.J. (2014). MacroH2A1.1 and PARP-1 cooperate to regulate transcription by promoting CBP-mediated H2B acetylation. Nat. Struct. Mol. Biol. *21*, 981–989. https://doi.org/10.1038/nsmb.2903.

Chen, H., Ruiz, P.D., McKimpson, W.M., Novikov, L., Kitsis, R.N., and Gamble, M.J. (2015). MacroH2A1 and ATM play opposing roles in paracrine senescence and the senescence-associated secretory phenotype. Mol. Cell *59*, 719–731. https://doi.org/10.1016/j.molcel.2015.07.011.

Creppe, C., Janich, P., Cantariño, N., Noguera, M., Valero, V., Musulén, E., Douet, J., Posavec, M., Martín-Caballero, J., Sumoy, L., et al. (2012). MacroH2A1 regulates the balance between self-renewal and differentiation commitment in embryonic and adult stem cells. Mol. Cell Biol. *32*, 1442–1452. https://doi.org/10.1128/mcb.06323-11.

Dardenne, E., Pierredon, S., Driouch, K., Gratadou, L., Lacroix-triki, M., Espinoza, M.P., Zonta, E., Germann, S., Mortada, H., Villemin, J.P., et al. (2012). Splicing switch of an epigenetic regulator by RNA helicases promotes tumor-cell invasiveness. Nat. Struct. Mol. Biol. *19*, 1139–1146. https://doi.org/10.1038/nsmb.2390.

Dell'Orso, S., Wang, A.H., Shih, H.-Y., Saso, K., Berghella, L., Gutierrez-Cruz, G., Ladurner, A.G., O'Shea, J., O'Shea, J.J., Sartorelli, V., and Zare, H. (2016). The histone variant MacroH2A1.2 is necessary for the activation of muscle enhancers and recruitment of the transcription factor Pbx1. Cell Rep. *14*, 1156–1168. https://doi.org/10.1016/j.celrep.2015.12.103.

Douet, J., Corujo, D., Malinverni, R., Renauld, J., Sansoni, V., Posavec-Marjanović, M., Cantariño, N., Valero, V., Mongelard, F., Bouvet, P., et al. (2017). MacroH2A histone variants maintain nuclear organization and heterochromatin architecture. J. Cell Sci. *130*, 1570–1582.

Durand, N.C., Shamim, M.S., Machol, I., Rao, S.S.P., Huntley, M.H., Lander, E.S., and Aiden, E.L. (2016). Juicer provides a one-click system for analyzing loop-resolution Hi-C experiments. Cell Syst. *3*, 95–98. https://doi.org/10.1016/j.cels.2016.07.002.

ENCODE Project Consortium; Dunham, I., Kundaje, A., Aldred, S.F., Collins, P.J., Davis, C.A., Doyle, F., Epstein, C.B., Frietze, S., Harrow, J., et al. (2013). An integrated encyclopedia of DNA elements in the human genome. Nature *489*, 57–74.

Fellmann, C., Hoffmann, T., Sridhar, V., Hopfgartner, B., Muhar, M., Roth, M., Lai, D.Y., Barbosa, I.A.M., Kwon, J.S., Guan, Y., et al. (2013). An optimized microRNA backbone for effective single-copy RNAi. Cell Rep. *5*, 1704–1713. https://doi.org/10.1016/j.celrep.2013.11.020.

Feng, H., Zhang, Y.B., Gui, J.F., Lemon, S.M., and Yamane, D. (2021). Interferon regulatory factor 1 (IRF1) and anti-pathogen innate immune responses. PLoS Pathog. *17*, e1009220. https://doi.org/10.1371/journal.ppat.1009220.

Filipescu, D., Hasson, D., Tung, N., Carcamo, S., Humblin, E., Goldberg, M., Vyas, N., Beaumont, K., Ghiraldini, F., Salmon, H., et al. (2022). MacroH2A restricts melanoma progression via inhibition of in ammatory gene expression in cancer-associated broblasts. Res. Square. https://doi.org/10.21203/rs.3.rs-1578023/v1.

Fishilevich, S., Nudel, R., Rappaport, N., Hadar, R., Plaschkes, I., Iny Stein, T., Rosen, N., Kohn, A., Twik, M., Safran, M., et al. (2017). GeneHancer: genome-wide integration of enhancers and target genes in GeneCards. Database *2017*, 1–17. https://doi.org/10.1093/database/bax028.

Galdiero, M.R., Marone, G., and Mantovani, A. (2018). Cancer inflammation and cytokines. Cold Spring Harb. Perspect. Biol. *10*, a028662. https://doi.org/10.1101/cshperspect.a028662.

Gamble, M.J., Frizzell, K.M., Yang, C., Krishnakumar, R., and Kraus, W.L. (2010). The histone variant macroH2A1 marks repressed autosomal chromatin, but protects a subset of its target genes from silencing. Genes Dev. *24*, 21–32. https://doi.org/10.1101/gad.1876110.

Garcia-Alonso, L., Holland, C.H., Ibrahim, M.M., Turei, D., and Saez-Rodriguez, J. (2019). Benchmark and integration of resources for the estimation of human transcription factor activities. Genome Res. *29*, 1363–1375. https://doi.org/10.1101/gr.240663.118.

Gaspar-Maia, A., Qadeer, Z.A., Hasson, D., Ratnakumar, K., Adrian Leu, N., Leroy, G., Liu, S., Costanzi, C., Valle-Garcia, D., Schaniel, C., et al. (2013). MacroH2A histone variants act as a barrier upon reprogramming towards pluripotency. Nat. Commun. *4*, 1565. https://doi.org/10.1038/ncomms2582.

Gel, B., and Serra, E. (2017). KaryoploteR: An R/Bioconductor package to plot customizable genomes displaying arbitrary data. Bioinformatics *33* (*19*), 3088–3090. https://doi.org/10.1093/bioinformatics/btx346.

Ghiraldini, F.G., Filipescu, D., and Bernstein, E. (2021). Solid tumours hijack the histone variant network. Nat. Rev. Cancer *21*, 257–275. https://doi.org/10.1038/s41568-020-00330-0.

Gocher, A.M., Workman, C.J., and Vignali, D.A.A. (2021). Interferon-γ: teammate or opponent in the tumour microenvironment? Nat. Rev. Immunol. *22*, 158–172. https://doi.org/10.1038/s41577-021-00566-3.

Goldman, M.J., Craft, B., Hastie, M., Repečka, K., McDade, F., Kamath, A., Banerjee, A., Luo, Y., Rogers, D., Brooks, A.N., et al. (2020). Visualizing and interpreting cancer genomics data via the Xena platform. Nat. Biotechnol. *38*, 675–678. https://doi.org/10.1038/s41587-020-0546-8.

Hanahan, D., and Weinberg, R.A. (2011). Hallmarks of cancer: the next generation. Cell *144*, 646–674. https://doi.org/10.1016/j.cell.2011.02.013.

Hernández-Muñoz, I., Lund, A.H., van der Stoop, P., Boutsma, E., Muijrers, I., Verhoeven, E., Nusinow, D.A., Panning, B., Marahrens, Y., and van Lohuizen, M. (2005). Stable X chromosome inactivation involves the PRC1 Polycomb complex and requires histone MACROH2A1 and the CULLIN3/SPOP ubiquitin E3 ligase. Proc. Natl. Acad. Sci. U S A *102*, 7635–7640. https://doi.org/10.1073/pnas.0408918102.

Hsu, C.J., Meers, O., Buschbeck, M., and Heidel, F.H. (2021). The role of macroh2a histone variants in cancer. Cancers *13*, 3003. https://doi.org/10.3390/cancers13123003.

Huang, Y., Liu, L., and Liu, A. (2018). Dickkopf-1: current knowledge and related diseases. Life Sci. *209*, 249–254. https://doi.org/10.1016/j.lfs.2018.08.019.

Hurtado-Bagès, S., Posavec Marjanovic, M., Valero, V., Malinverni, R., Corujo, D., Bouvet, P., Lavigne, A.C., Bystricky, K., and Buschbeck, M. (2020). The histone variant MacroH2A1 regulates key genes for myogenic cell fusion in a splice-isoform dependent manner. Cells *9*, 1109. https://doi.org/10.3390/cells9051109.

Jiang, P., Freedman, M.L., Liu, J.S., and Liu, X.S. (2015). Inference of transcriptional regulation in cancers. Proc. Natl. Acad. Sci. U S A *112*, 7731–7736. https://doi.org/10.1073/pnas.1424272112.

Kapoor, A., Goldberg, M.S., Cumberland, L.K., Ratnakumar, K., Segura, M.F., Emanuel, P.O., Menendez, S., Vardabasso, C., Leroy, G., Vidal, C.I., et al. (2010). The histone variant macroH2A suppresses melanoma progression through regulation of CDK8. Nature *468*, 1105–1109. https://doi.org/10.1038/nature09590.

Kim, J., Shin, Y., Lee, S., Kim, M., Punj, V., Lu, J.F., Shin, H., Kim, K., Ulmer, T.S., Koh, J., et al. (2018a). Regulation of breast cancer-induced osteoclastogenesis by MacroH2A1.2 involving EZH2-mediated H3K27me3. Cell Rep. *24*, 224–237. https://doi.org/10.1016/j.celrep.2018.06.020.

Kim, J.M., Shin, Y., Lee, S., Kim, M.Y., Punj, V., Shin, H.I., Kim, K., Koh, J.M., Jeong, D., and An, W. (2018b). MacroH2A1.2 inhibits prostate cancer-induced osteoclastogenesis through cooperation with HP1α and H1.2. Oncogene *37*, 5749–5765. https://doi.org/10.1038/s41388-018-0356-3.

Kozlowski, M., Corujo, D., Hothorn, M., Guberovic, I., Mandemaker, I.K., Blessing, C., Sporn, J., Gutierrez-Triana, A., Smith, R., Portmann, T., et al. (2018). MacroH2A histone variants limit chromatin plasticity through two distinct mechanisms. EMBO Rep. *19*, e44445. https://doi.org/10.15252/embr.201744445.

Lavigne, A.-C., Castells, M., Mermet, J., Kocanova, S., Dalvai, M., and Bystricky, K. (2014). Increased macroH2A1.1 expression correlates with poor survival of triple-negative breast cancer patients. PLoS One *9*, e98930. https://doi.org/10.1371/journal.pone.0098930.

Lavigne, M.D., Vatsellas, G., Polyzos, A., Mantouvalou, E., Sianidis, G., Maraziotis, I., Agelopoulos, M., and Thanos, D. (2015). Composite macroH2A/NRF-1 nucleosomes suppress noise and generate robustness in gene expression. Cell Rep. *11*, 1090–1101. https://doi.org/10.1016/j.celrep.2015.04.022.

Leroy, G., Dimaggio, P.A., Chan, E.Y., Zee, B.M., Blanco, M.A., Bryant, B., Flaniken, I.Z., Liu, S., Kang, Y., Trojer, P., et al. (2013). A quantitative atlas of histone modification signatures from human cancer cells. Epigenet. Chromatin *6*, 20. https://doi.org/10.1186/1756-8935-6-20.

López-Terrada, D., Cheung, S.W., Finegold, M.J., and Knowles, B.B. (2009). Hep G2 is a hepatoblastoma-derived cell line. Hum. Pathol. *40*, 1512–1515. https://doi.org/10.1016/j.humpath.2009.07.003.

Love, M.I., Huber, W., and Anders, S. (2014). Moderated estimation of fold change and dispersion for RNA-seq data with DESeq2. Genome Biol. *15*, 550.

Liberzon, A., Birger, C., Thorvaldsdóttir, H., Ghandi, M., Mesirov, J.P., and Tamayo, P. (2015). The Molecular Signatures Database Hallmark Gene Set Collection. Cell Syst. *1* (*6*), 417–425. https://doi.org/10.1016/j.cels.2015.12.004.

Lo Re, O., Fusilli, C., Rappa, F., Van Haele, M., Douet, J., Pindjakova, J., Rocha, S.W., Pata, I., Valčíková, B., Uldrijan, S., et al. (2017). Induction of cancer cell stemness by depletion of macrohistone H2A1 in hepatocellular carcinoma. Hepatology *67*, 636–650. https://doi.org/10.1002/hep.29519.

Lo Re, O., Mazza, T., Giallongo, S., Sanna, P., Rappa, F., Vinh Luong, T., Li Volti, G., Drovakova, A., Roskams, T., van Haele, M., et al. (2020). Loss of histone macroH2A1 in hepatocellular carcinoma cells promotes paracrine-mediated chemoresistance and CD4+CD25+FoxP3+ regulatory T cells activation. Theranostics *10*, 910–924. https://doi.org/10.7150/thno.35045.

Malladi, S., MacAlinao, D.G., Jin, X., He, L., Basnet, H., Zou, Y., De Stanchina, E., and Massagué, J. (2016). Metastatic latency and immune evasion through autocrine inhibition of WNT. Cell *165*, 45–60. https://doi.org/10.1016/j.cell.2016.02.025.

Mallona, I., Díez-Villanueva, A., Martín, B., and Peinado, M.A. (2017). Chainy: an universal tool for standardized relative quantification in real-time PCR. Bioinformatics *33*, 1411–1413. https://doi.org/10.1093/bioinformatics/btw839.

Martire, S., and Banaszynski, L.A. (2020). The roles of histone variants in fine-tuning chromatin organization and function. Nat. Rev. Mol. Cell Biol. *21*, 522–541. https://doi.org/10.1038/s41580-020-0262-8.

Morgenstern, J.P., and Land, H. (1990). Advanced mammalian gene transfer: high titre retroviral vectors with multiple drug selection markers and a complementary helper-free packaging cell line. Nucleic Acids Res. *18*, 3587–3596. https://doi.org/10.1093/nar/18.12.3587.

Mumbach, M.R., Rubin, A.J., Flynn, R.A., Dai, C., Khavari, P.A., Greenleaf, W.J., and Chang, H.Y. (2016). HiChIP: efficient and sensitive analysis of protein-directed genome architecture. Nat. Methods *13*, 919–922. https://doi.org/10.1038/nmeth.3999.

Ouararhni, K., Hadj-Slimane, R., Ait-Si-Ali, S., Robin, P., Mietton, F., Harel-Bellan, A., Dimitrov, S., and Hamiche, A. (2006). The histone variant mH2A1.1 interferes with transcription by down-regulating PARP-1 enzymatic activity. Genes Dev. *20*, 3324–3336. https://doi.org/10.1101/gad.396106.

Pasque, V., Gillich, A., Garrett, N., and Gurdon, J.B. (2011). Histone variant macroH2A confers resistance to nuclear reprogramming. EMBO J. *30*, 2373–2387. https://doi.org/10.1038/emboj.2011.144.

Patro, R., Duggal, G., Love, M.I., Irizarry, R.A., and Kingsford, C. (2017). Salmon provides fast and bias-aware quantification of transcript expression. Nat. Methods *14*, 417–419. https://doi.org/10.1038/nmeth.4197.

Perkins, N.D. (2012). The diverse and complex roles of NF-κB subunits in cancer. Nat. Rev. Cancer *12*, 121–132. https://doi.org/10.1038/nrc3204.

Perkins, J.R., Dawes, J.M., McMahon, S.B., Bennett, D.L.H., Orengo, C., and Kohl, M. (2012). ReadqPCR and NormqPCR: R packages for the reading, quality checking and normalisation of RT-qPCR quantification cycle (Cq) data. BMC Genom. *13*, 296. https://doi.org/10.1186/1471-2164-13-296.

Posavec, M., Timinszky, G., and Buschbeck, M. (2013). Macro domains as metabolite sensors on chromatin. Cell. Mol. Life Sci. *70*, 1509–1524. https://doi.org/10.1007/s00018-013-1294-4.

Ramos-Rodríguez, M., Subirana-Granés, M., and Pasquali, L. (2021). UMI4Cats: an R package to analyze chromatin contact profiles obtained by UMI-4C. Bioinformatics, 1–3. https://doi.org/10.1093/bioinformatics/btab392.

Ratnakumar, K., Duarte, L.F., LeRoy, G., Hasson, D., Smeets, D., Vardabasso, C., Bönisch, C., Zeng, T., Xiang, B., Zhang, D.Y., et al. (2012). ATRX-mediated chromatin association of histone variant macroH2A1 regulates α-globin expression. Genes Dev. *26*, 433–438. https://doi.org/10.1101/gad.179416.111.

Ritchie, M.E., Phipson, B., Wu, D., Hu, Y., Law, C.W., Shi, W., and Smyth, G.K. (2015). Limma powers differential expression analyses for RNA-sequencing and microarray studies. Nucleic Acids Res. *43*, e47. https://doi.org/10.1093/nar/gkv007.

Ritz, C., and Spiess, A.N. (2008). qpcR: an R package for sigmoidal model selection in quantitative real-time polymerase chain reaction analysis. Bioinformatics *24*, 1549–1551. https://doi.org/10.1093/bioinformatics/btn227.

Roadmap Epigenomics Consortium; Kundaje, A., Meuleman, W., Ernst, J., Bilenky, M., Yen, A., Heravi-Moussavi, A., Kheradpour, P., Zhang, Z., Ziller, M.J., Wang, J., et al. (2015). Integrative analysis of 111 reference human epigenomes. Nature *518*, 317–330. https://doi.org/10.1038/nature14248.

Schnater, J.M., Köhler, S.E., Lamers, W.H., Von Schweinitz, D., and Aronson, D.C. (2003). Where do we stand with hepatoblastoma? A review. Cancer *98*, 668–678. https://doi.org/10.1002/cncr.11585.

Schubert, M., Klinger, B., Klünemann, M., Sieber, A., Uhlitz, F., Sauer, S., Garnett, M.J., Blüthgen, N., and Saez-Rodriguez, J. (2018). Perturbation-response genes reveal signaling footprints in cancer gene expression. Nat. Commun. *9*, 20. https://doi.org/10.1038/s41467-017-02391-6.

Schwartzman, O., Mukamel, Z., Oded-Elkayam, N., Olivares-Chauvet, P., Lubling, Y., Landan, G., Izraeli, S., and Tanay, A. (2016). UMI-4C for quantitative and targeted chromosomal contact profiling. Nat. Methods *13*, 685–691. https://doi.org/10.1038/nmeth.3922.

Soneson, C., Love, M.I., and Robinson, M.D. (2016). Differential analyses for RNA-seq: transcript-level estimates improve gene-level inferences. F1000Research *4*, 1521. https://doi.org/10.12688/f1000research.7563.2.

Stovner, E.B., and Sætrom, P. (2019). Epic2 efficiently finds diffuse domains in ChIP-seq data. Bioinformatics *35*, 4392–4393. https://doi.org/10.1093/bioinformatics/btz232.

Subramanian, A., Tamayo, P., Mootha, V.K., Mukherjee, S., and Ebert, B.L. (2005). Gene set enrichment analysis : a knowledge-based approach for interpreting genome-wide. Proc. Natl. Acad. Sci. U S A *102*, 15545–15550.

Sun, Z., Filipescu, D., Andrade, J., Gaspar-Maia, A., Ueberheide, B., and Bernstein, E. (2018). Transcription-associated histone pruning demarcates macroH2A chromatin domains. Nat. Struct. Mol. Biol. *25*, 958–970. https://doi.org/10.1038/s41594-018-0134-5.

Taniguchi, K., and Karin, M. (2018). NF-κB, inflammation, immunity and cancer: coming of age. Nat. Rev. Immunol. *18*, 309–324. https://doi.org/10.1038/nri.2017.142.

Timinszky, G., Till, S., Hassa, P.O., Hothorn, M., Kustatscher, G., Nijmeijer, B., Colombelli, J., Altmeyer, M., Stelzer, E.H.K., Scheffzek, K., et al. (2009). A macrodomain-containing histone rearranges chromatin upon sensing PARP1 activation. Nat. Struct. Mol. Biol. *16*, 923–929. https://doi.org/10.1038/nsmb.1664.

Weinstein, J.N., Collisson, E.A., Mills, G.B., Shaw, K.R.M., Ozenberger, B.A., Ellrott, K., Shmulevich, I., Stuart, J.M., Chang, K., Creighton, C.J., et al. (2013). The cancer genome atlas pan-cancer analysis project. Nat. Genet. *45*, 1113–1120. https://doi.org/10.1038/ng.2764.

Wickham, H. (2016). ggplot2: Elegant Graphics for Data Analysis (Springer-Verlag New York).

Wingett, S., Ewels, P., Furlan-Magaril, M., Nagano, T., Schoenfelder, S., Fraser, P., and Andrews, S. (2015). HiCUP: pipeline for mapping and processing Hi-C data. F1000Research, 1310. https://doi.org/10.12688/f1000research.7334.1.

Wu, T., Hu, E., Xu, S., Chen, M., Guo, P., Dai, Z., Feng, T., Zhou, L., Tang, W., Zhan, L., et al. (2021). clusterProfiler 4.0: a universal enrichment tool for interpreting omics data. Innovation *2*, 100141. https://doi.org/10.1016/j.xinn.2021.100141.

Yardımcı, G.G., Ozadam, H., Sauria, M., Ursu, O., Yan, K.-K., Yang, T., Chakraborty, A., Kaul, A., Lajoie, B., Song, F., et al. (2017). Measuring the reproducibility and quality of Hi-C data. Genome Biol. *20*, 57.

Zelová, H., and Hošek, J. (2013). TNF-α signalling and inflammation: interactions between old acquaintances. Inflamm. Res. *62*, 641–651. https://doi.org/10.1007/s00011-013-0633-0.

STAR★METHODS

KEY RESOURCES TABLE

REAGENT or RESOURCE	SOURCE	IDENTIFIER
Antibodies		
anti-macroH2A1	(Buschbeck et al., 2009; Douet et al., 2017)	N/A
anti-macroH2A2	(Douet et al., 2017)	N/A
anti-DKK1	Santa Cruz Biotechnology	Cat#sc-374574; RRID: AB_10989416
anti-FLAG	Sigma-Aldrich	Cat#F1804; RRID:AB_262044
anti-H3	Abcam	Cat#ab1791; RRID:AB_302613
anti-H3K4me3	Abcam	Cat#ab8580; RRID:AB_306649
anti-H3K27Ac	Abcam	Cat#ab4729; RRID:AB_2118291
anti-IgG	Abcam	Cat#ab46540; RRID:AB_2614925
IRDye 680RD Goat anti-Rabbit IgG Secondary Antibody	LI-COR Biosciences	Cat# 926-68071, RRID:AB_10956166
IRDye 680RD Goat anti-Mouse IgG	LI-COR Biosciences	Cat# 926-68070, RRID:AB_10956588
IRDye 800CW Goat anti-Rabbit IgG	LI-COR Biosciences	Cat# 926-32211, RRID:AB_621843
IRDye 800CW Goat anti-Mouse IgG	LI-COR Biosciences	Cat# 926-32210, RRID:AB_621842
Goat Anti-Rabbit Immunoglobulins/HRP	Dako	P0448
Goat Anti-Mouse Immunoglobulins/HRP	Dako	P0447
Chemicals, peptides, and recombinant proteins		
Dulbecco's modified Eagle medium (DMEM)	Thermo Fisher Scientific	Cat# 11960085
Fetal Bovine Serum	Thermo Fisher Scientific	Cat# 10270106
L-Glutamine (200mM)	Thermo Fisher Scientific	Cat# 25030024
Penicillin-Streptomycin (10,000 U/mL)	Thermo Fisher Scientific	Cat# 15140122
Recombinant Human TNF-α	Peprotech	Cat# 300-01A
Recombinant Human IFN-γ	Peprotech	Cat# 300-02
BMS-345541	Abcam	Cat# ab144822
Matrigel Matrix	Corning	Cat# 354234
DpnII	New England Biolabs	Cat# 174R0543M
T4 ligase	Promega	Cat# M1804
Critical commercial assays		
Maxwell RSC simplyRNA Cells Kit	Promega	Cat# AS1390
Pierce ECL Western Blotting Substrate	Thermo Fisher Scientific	Cat# 32106
TRIzol Reagent	Thermo Fisher Scientific	Cat# 15596026
First Strand cDNA Synthesis Kit	Thermo Fisher Scientific	Cat# K1612
LightCycler® 480 SYBR Green I Master	Roche	Cat# 04707516001
Magna ChIP™ Protein A+G Magnetic Beads	Merck	Cat# 16-663
ChIP DNA Clean & Concentrator	Zymo Research	Cat# D5205
Qubit™ dsDNA HS	Thermo Fisher Scientific	Cat# Q32851
Deposited data		
RNA-Seq, HiChIP and UMI-4C	This paper	GSE161859
RNA-Seq from 32 patients with hepatoblastoma	(Carrillo-Reixach et al., 2020)	GSE133039
ChIP-Seq of macroH2A1 and macroH2A2 in HepG2	(Douet et al., 2017)	GSE58175
ChIP-Seq of H3K27Ac in HepG2	ENCODE (ENCODE Project Consortium et al., 2013)	GEO:GSM733743

(*Continued on next page*)

Continued

REAGENT or RESOURCE	SOURCE	IDENTIFIER
ChIP-Seq of RELA in HepG2	ENCODE (ENCODE Project Consortium et al., 2013)	GSE170794
HiC in HepG2	ENCODE (ENCODE Project Consortium et al., 2013)	ENCSR194SRI
GeneHancer Database	(Fishilevich et al., 2017)	N/A
refTSS	(Abugessaisa et al., 2019)	N/A
HMM Chromatin Segmentation (Core 15-state model)	(Roadmap Epigenomics Consortium et al., 2015)	N/A
TCGA Pan-Cancer Batch effects normalized mRNA data	(Weinstein et al., 2013), accessed through the UCSC Xena Browser (Goldman et al., 2020)	EB++AdjustPANCAN_IlluminaHiSeq_ RNASeqV2.geneExp.xena
TCGA Pan-Cancer RABIT transcription factor regulatory impact, HiSeqV2	(Jiang et al., 2015), accessed through the UCSC Xena Browser (Goldman et al., 2020)	RABIT/pancan/RABIT_pancan.HiSeq.V2
Molecular Signatures Database	(Liberzon et al., 2015)	MSigDB v7.2
Experimental models: Cell lines		
HepG2	ATCC	Cat#HB-8065; RRID:CVCL_0027
Experimental models: Organisms/strains		
NOD.CB17-PRKDC^{SCID} Mouse	Charles River Laboratories	Strain code:394
Oligonucleotides		
For a list of all primers used see Table S2	This paper	N/A
Recombinant DNA		
pBabe.puro	(Morgenstern and Land, 1990)	Addgene# 1764
pBabe.puro – FLAG-mH2A1.2	This paper	N/A
pBabe.puro – FLAG-mH2A2	This paper	N/A
SGEP	(Fellmann et al., 2013)	Addgene# 111170
SGEP - sh Renilla	This paper	N/A
SGEP - sh mH2A1	This paper	N/A
SGEP - sh mH2A2	This paper	N/A
Software and algorithms		
Salmon	(Patro et al., 2017)	RRID:SCR_017036
DESeq2	(Love et al., 2014)	RRID:SCR_015687
tximport	(Soneson et al., 2016)	RRID:SCR_016752
limma	(Ritchie et al., 2015)	RRID:SCR_010943
GSEA v4.03 for Mac	(Subramanian et al., 2005)	RRID:SCR_003199
clusterProfiler	(Wu et al., 2021)	RRID:SCR_016884
PROGENy	(Schubert et al., 2018)	N/A
VIPER	(Alvarez et al., 2016)	N/A
DoRothEA	(Garcia-Alonso et al., 2019)	RRID:SCR_005569
Juicer	(Durand et al., 2016)	RRID:SCR_017226

RESOURCE AVAILABILITY

Lead contact

Further information and requests for resources and reagents should be directed to and will be fulfilled by the lead contact, Marcus Buschbeck (mbuschbeck@carrerasresearch.org).

Materials availability

All unique/stable reagents generated in this study are available from the lead contact with a completed Materials Transfer Agreement (MTA).

Data and code availability

- The RNA-Seq, HiChIP and UMI-4C data generated and analyzed for this study has been deposited in the Gene Expression Omnibus and are publicly available as of the date of publication. Accession numbers are listed in the key resources table.
- This paper analyzes existing, publicly available data. The accession numbers for the datasets are listed in the key resources table.
- This paper does not report original code.
- Any additional information required to reanalyze the data reported in this paper is available from the lead contact upon request.

EXPERIMENTAL MODEL AND SUBJECT DETAILS

Cell lines

HepG2 cells (ATCC, HB-8065) were routinely cultured in Dulbecco's modified Eagle medium (DMEM) containing 4.5 g/L glucose (Gibco) supplemented with 10% v/v fetal bovine serum (FBS) (Gibco), 2 mM L-glutamine (Gibco), 50 U/mL penicillin (Gibco) and 50 mg/mL streptomycin (Gibco) at 37°C in 5% CO_2.

Animals

Four weeks old NOD.CB17-PRKDC^{SCID} immunosuppressed mice were purchased from Charles River Laboratories (strain code 394). The animals were kept in specific pathogen free (SPF) conditions for the duration of the experiment. The animals were kept in the stall for two weeks before the experimental procedure. Three male and two female animals were used for each experimental group. The Animal Experimentation Commission of the Catalan Government (Comissó d'Experimentació Animal de la Generalitat de Catalunya) has approved the animal experimentation procedures performed in this study with project reference 9500.

METHOD DETAILS

Cloning of plasmids

All cloning procedures were performed following standard cloning techniques involving PCR amplification, restriction enzyme digestion and ligation reactions. Full-length FLAG-tagged mouse macroH2A1.2 and macroH2A2 were generated by cloning the PCR amplified cDNA of mouse macroH2A2 into a pCMV-Tag2A and then subcloning into a pBabe.puro backbone. Short-hairpin RNA sequences were cloned into pRRL-SFFV-GFP- miRE-PGK-Puro (SGEP) vectors as described (Fellmann et al., 2013).

Cell lines, culture condition, gene transduction and treatments

HepG2 cell lines with a stable shRNA-mediated double knock-down of macroH2A1 and macroH2A2 (DKD) and their random sequence control counterparts (CTL) have been described previously (Douet et al., 2017). HepG2 cells (ATCC, HB-8065) were routinely cultured in Dulbecco's modified Eagle medium (DMEM) containing 4.5 g/L glucose (Gibco) supplemented with 10% v/v fetal bovine serum (FBS) (Gibco), 2 mM L-glutamine (Gibco), 50 U/mL penicillin (Gibco) and 50 mg/mL streptomycin (Gibco) at 37°C in 5% CO_2. Stable cell lines were generated by transduction of viral vectors selected as previously described (Cantariño et al., 2016). pRRL-SFFV-GFP- miRE-PGK-Puro (SGEP, Fellmann et al., 2013)) vectors encoding either a shRNA cassette against transcripts of Renilla (non-targeting control), mH2A1 or mH2A2 were used for transduction to generate stable single knock-downs in HepG2.

The following procedure was followed to treat the cells with TNFα or IFNγ: 500.000 HepG2 cells were seeded in six-well plates and incubated overnight in standard conditions. Cells were starved of FBS over night by reducing its concentration to 0.5%. After that, TNFα or IFNγ (PeproTech, resuspended in PBS 0.1% BSA) was added to the media to a final concentration of 20 ng/mL or 100ng/mL, respectively (or at different concentrations if indicated in the figure). An equal volume of PBS 0.1% BSA was added as the untreated control condition. The cells were treated for 24h with TNFα and 48h with IFNγ, then collected and subject to protein and RNA expression analysis. The same procedure was followed when evaluating the effect of the IKK inhibitor BMS-345541 (Abcam, resuspended in DMSO) with the following modifications: 150.000 cells were seeded in 12-well plates, the inhibitor was added at a final concentration of 2 μM 1h prior to adding TNFα and an equal volume of DMSO was used as the untreated control condition. To obtain samples for ChIP experiments, the same treatment protocol was followed but 10 million cells were seeded in P15 plates and grown for two days before applying the o/n serum starvation, subsequent TNFα treatment and fixation after 24h.

Xenografts

The Animal Experimentation Commission of the Catalan Government (Comissó d'Experimentació Animal de la Generalitat de Catalunya) has approved animal experimentation procedure used for the xenograft experiment with project reference 9500. Four weeks old NOD.CB17-PRKDC^{SCID} immunosuppressed mice were purchased from Charles Rivers Laboratories (strain code 394). The animals were kept in specific pathogen free (SPF) conditions for the duration of the experiment. The animals were kept in the stall for two weeks before the experimental procedure. CTL and DKD HepG2 cells were resuspended in a Matrigel (Corning) and PBS mix 1:1. The animals were anesthesiated with isofluorane and two subcutaneous injections were performed in each lower flank of the animal consisting of 100 μL Matrigel:PBS 1:1 containing 5 million cells. A total of 5 mice (three males, two females) per condition was

used, effectively resulting in 10 injections for each cell line. The weight and overall condition of the mice were regularly monitored. The tumor size was monitored every 2-3 days and measured with a digital caliper. Two measurements were performed for each tumor approximating the longer (*a*) and shorter (*b*) axis of an ellipse fitted to the tumor and the tumor volume was estimated by calculating $(a \times b)^2/2$. 21 days after the injection, tumors were resected with the mice under anesthesia and all animals were sacrificed. Tumors were cleaned with PBS and cut in half. One half was fixed in formalin and embedded in paraffin for histological analysis, while the other half was immediately frozen in liquid nitrogen for later RNA extraction.

Immunoblotting

Protein extraction was performed by resuspending cell pellets Laemmli's buffer. After heating at 95°C for 10 min, the samples were analyzed by Western blot. Samples were loaded on 12% polyacrylamide gels and run at 36 mA for 45-60 min to achieve optimal separation and then transferred at 220 mA for 90 min onto a nitrocellulose membrane (GE healthcare). After transfer, protein load was checked by Ponceau staining and the membranes were blocked using 5% non-fat milk (Nestlé) in TBST for 15 min. Membranes were incubated with primary antibodies o/n at 4°C. The day after, membranes were washed thrice with TBST for 10 min and incubated for 1 h at RT with either Fluorophore-conjugated secondary antibodies (Figure 5B, LI-COR Biosciences IRDye 680RD and IRDye 800CW) or HRP-conjugated antibodies (Figure 1A, DakoCytomation). Membranes were then washed again thrice with TBST for 10min. For the detection of fluorescent signals, the dried membranes were scanned with an Odyssey® CLx Imager. For the detection of chemiluminescent signals, the membranes were incubated 1 min with Pierce™ ECL Western Blotting Substrate (Thermo Scientific) chemiluminescent reagent mix in a 1:1 ratio. Dried membranes were overlaid with photographic film (GE Healthcare) for a few seconds up to 5 min to achieve proper exposures and the films were developed with a FujiFilm FPM-100A developer.

For the detection of secreted proteins, 1 mL of culture media was collected and used for acetone precipitation of extracellular proteins. First, the sample was briefly centrifuged to remove any detached cells that might be in suspension. Then, four volumes of cold (−20°C) acetone were added to the tube. After vortexing, the sample was incubated o/n at −20°C. The sample was centrifuged 10min at 13000g and the supernatant was discarded. The protein pellet was air-dried at room temperature for 30 min and.

RNA isolation and gene expression analysis by RT-qPCR

Cultured cells were collected by trypsinization and washed twice with PBS. Total RNA was isolated using the Maxwell® RSC simplyRNA Cells Kit (Promega) together with the Maxwell® RSC Instrument (Promega) according to the manufacturer's instructions. Total RNA from xenograft samples was isolated using the TRIzol™ Reagent (ThermoFisher Scientific). Concentration and quality of the extracted RNA was checked using a Nanodrop instrument (Thermo Scientific).

For quantitative PCR after reverse transcription (RT-qPCR), 1 μg of total RNA was used for cDNA synthesis using the First Strand cDNA synthesis kit (Thermo Scientific) according to the manufacturer's instructions. Resulting cDNAs were diluted 10 fold in autoclaved ddH_2O previous to real-time PCR analysis using a LightCycler® 480 II instrument (Roche). A 10 μL reaction mix containing 5 μL LightCycler® 480 SYBR Green I Master (Roche), 0.5 μL of forward and reverse primers (for a final concentration of 1 μM), 2 μL of diluted cDNA and 2 μL of autoclaved ddH_2O was loaded in 384-well plates.

The median efficiency of each primer pair was determined in every RT-qPCR plate run using the software *chainy* (Mallona et al., 2017) that is based on the R packages *qpcR* and *NormqPCR* (Perkins et al., 2012; Ritz and Spiess, 2008). The expression of a target RNA in a sample relative to a control sample was calculated using a variation of the ΔCt method that accounts for the efficiency of the primers as follows: $efficiency_{target}^{(Ct_{control} - Ct_{sample})}$. All values were normalized by the average expression of two reference genes: GAPDH and RPLP0. The normalized relative expression value is used in all the plots and statistics. All quantifications of RNA expression are relative, so that the chosen control sample will have an expression of 1 for all target genes and the rest of the samples will have an expression that represents a multiple or fraction of the expression in the control.

Transcriptomic analysis

One microgram of total RNA was submitted to the Genomics Unit of the Centre for Genomic Regulation (Barcelona, Spain) who prepared the libraries with a poly(A) selection and sequenced them in an Illumina HiSeq2500 using 50bp single reads obtaining >30M reads per sample. Five different samples of each X.CTL and X.DKD and three replicates of CTL and DKD untreated or treated with TNFα were sequenced. To quantify the transcript expression we used *Salmon* (Patro et al., 2017) version 0.14.0, using *libtype A* and the *validateMappigs* option active. The raw reads were "quasi-aligned" to the human Ensembl genome annotation GRCh38.12. The quantification results obtained from *Salmon* were imported to the *DESeq2* R package (Love et al., 2014) using the *tximport* R package (Soneson et al., 2016). For the xenograft samples, the design formula for DESeq2 included only the type of tumor as a variable (X.CTL or X.DKD) and the contrast X.DKD vs X.CTL was applied using the *results* function to obtain log2FC and p-values. For the cultured HepG2 cells samples, the experimental groups were defined as a combination of cell line and treatment, resulting in four groups: CTL untreated, DKD untreated, CTL + TNFα and DKD + TNFα. The design formula for DESeq2 included the experimental group plus the experimental replicate. The variance-stabilized log2 gene expression values were extracted using the *rlog* or *vst* functions (for HepG2 and hepatoblastoma datasets, respectively), which minimizes differences between samples for rows with small counts. For the analysis of normal liver tissue and hepatoblastoma tumor expression, the variance-stabilized log2 expression values of MACROH2A1 were used to classify the tumor

samples in 3 quantiles. The quantile annotation was used as design formula for *DESeq2* and the contrast between the lowest and highest mH2A1 expression quantiles was performed. Specific contrasts where extracted as indicated in each figure to obtain log2FC and p-values using the *lfcShrink* function with the *ashr* type of log2FC shrinkage. The *removeBatchEffect* function from the *limma* R package (Ritchie et al., 2015) was used on the log2 expression matrix to reduce the variability explained by different experimental replicates for the purposes of Principal Component Analysis, sample distances calculation and log2 gene expression plotting. Ensembl Gene IDs where mapped to HGNC symbols whenever possible, otherwise the Ensembl Gene ID was kept as annotation. In all cases, genes with a Benjamini-Hochberg adjusted p-value lower than 0.05 were selected as being significantly differentially expressed.

Enrichment analysis of gene sets and gene ontologies

Differentially expressed gene lists with an HGNC annotation were ranked by log2FC value for a Gene Set Enrichment Analysis (GSEA) using the pre-ranked functionality of the *GSEA* software (Subramanian et al., 2005) (v4.03 for Mac). As gene database we selected the hallmark gene sets from the Molecular Signatures Database (MSigDB v7.2 updated September 2020) (Liberzon et al., 2015) which contains gene expression signatures derived by aggregating many MSigDB gene sets to represent well-defined biological states or processes.

For gene ontology enrichment analysis, the function *enrichGO* from the R package *clusterProfiler* (Wu et al., 2021) was used, with *minGSS* = 20 and an adjusted p-value cut-off of 0.05. Enriched categories were ranked according to the number of differentially expressed genes and a subset of the top categories listed was plotted in the figures.

Inference of pathway and transcription factor activity from transcriptomic data

We used the R package PROGENy (Schubert et al., 2018) on the rlog variance-stabilized gene expression matrices to calculate pathway activity scores per sample according to the top 100 genes of each pathway. After scaling the pathway scores to the control samples, we applied a linear model to identify the pathways significantly different between experimental groups (pv of the estimate coefficient < 0.05). We used the R packages *VIPER* (Alvarez et al., 2016) and *DoRothEA* (Garcia-Alonso et al., 2019) to evaluate regulon activity from gene expression data. For Figures 6 and S2, the ranked log2FC of differentially expressed genes was used as input for *msVIPER* with regulons of the highest confidence (A). For Figure 5, The normalized gene expression counts were extracted using *DESeq2* function *counts* and used as input for VIPER as implemented in the wrapper function *run_viper* in *DoRothEA* with the parameters *method = "scale"*, *minsize = 4* and *eset.filter = FALSE* and the two regulons of most confidence (A, B). A two-tailed Student's t-test was performed and TFs with an adjusted p-value (Bonferroni-Hochberg) less than 0.05 were considered to have significantly different inferred activity between the experimental groups.

Chromatin immunoprecipitation

Between 20 and 30 million HepG2 cells were fixed with a PBS solution containing 1% FA for 10 min at RT. The fixation was quenched by the addition of glycine to a concentration of 0.125M and incubation for 5 min at RT. Cells were then washed with cold PBS and scraped off the plate. Nuclei extraction was achieved by resuspending the fixed cells in 500 μL lysis buffer I (5 mM PIPES pH 8, 85 mM KCl, 0.5% NP-40, 1 mM PMSF, 50 μg/mL leupeptin) and incubating for 30min at 4°C in rotation. Lysed cells were centrifuged at 5000 rpm for 5 min at 4°C, the supernatant was discarded and the pellet resuspended in 500 μL lysis buffer II (1% SDS, 10 mM EDTA pH 8, 50 mM TRIS pH 8, 1 mM PMSF, 50 μg/mL leupeptin) and incubated for 30min at 4°C in rotation. Chromatin shearing was achieved by sonication in a Bioruptor® Pico (Diagenode, 10 cycles 30sec ON/30 sec OFF at high intensity). Samples were then centrifuged for 10 min at 10000rpm to remove insoluble debris and a 10 μL aliquot of lysate was purified, quantified and run on an agarose gel to test the size range after sonication. 35 μg of sheared chromatin were used for each immunoprecipitation (IP) reaction diluted with 9 volumes of IP dilution buffer (1% Triton X-100, 150 mM NaCl, 2 mM EDTA pH 8, 20 mM TRIS pH 8, 1mM PMSF). Samples were precleared with 20 μL of Magna ChIP™ protein A/G magnetic beads (Merck Millipore) for 2 h at 4°C in rotation. 10% of the precleared lysate was taken as input. Antibodies were added to each IP and samples were incubated o/n at 4°C in rotation. The following day 20 μL of Magna ChIP™ protein A/G magnetic beads (Merck Millipore) were added to capture the antibody-bound chromatin fraction for 2 h at 4°C in rotation. Beads were washed twice at RT with each of the following buffers in this order: mixed micelle was buffer (140 mM NaCl, 20 mM Tris-HCl pH 8, 5 mM EDTA pH 8, 5% sucrose w/v, 1% Triton X-100 v/v, 0.2% SDS, 0.02% NaN3), LiCl/detergent wash (0.5% deoxycholic acid sodium salt w/v, 1 mM EDTA, 250 mM LiCl, 0.5% NP-40 v/v, 10 mM Tris-HCl pH 8), buffer 500 (0.1% deoxycholic acid sodium salt w/v, 1mM EDTA, 50mM HEPES pH 7.5, 500 mM NaCl, 1% Triton X-100 v/v, 0.02% NaN3) and TE buffer (10mM Tris-HCl pH8, 1 mM EDTA pH 8). The enriched chromatin was eluted by resuspending the beads in 200 μL of elution buffer (1%SDS, 100 mM NaHCO3), 30 sec of vortexing and incubation for 30 min at RT in rotation. Two sequential elutions were performed and the eluates were combined. The input samples were included again in the experimental procedure at this point. Crosslinking reversal was achieved by adding NaCl to a final concentration of 200 mM and incubating the samples o/n at 65°C shaking. The following day the protein in the samples was digested by adding 2 μL of Proteinase K 10 mg/mL, 16 μL 1M TRIS pH 6.5 and 8 μL 500 mM EDTA and incubating for 2 h at 45°C. ChIP DNA was purified using ChIP DNA Clean & Concentrator (Zymo Research) and analyzed by qPCR in a similar way to the "Gene expression analysis by RT-qPCR" description. The input of each sample was used as the "control" sample to obtain a relative enrichment over input, using the same formula than for RNA expression.

The relative enrichment was then converted to a percentage. The percentage of input value divided by the signal of the H3 ChIP is used in the ChIP plots.

UMI-4C

UMI-4C was performed essentially following a described protocol (Schwartzman et al., 2016). More specifically, 2.5 million HepG2 cells were seeded in 6-well plates. The day after, the cells were fixed by addition of PBS 1% FA and incubation for 10 min at RT. The reaction was stopped by adding glycine to a final concentration of 0.125M and incubation for 5 min on ice. The cells were then collected by scraping, washed with PBS and resuspended in 500 μL of lysis buffer (10 mM TRIS pH 8, 10 mM NaCl, 0.2% NP-40) and incubated for 30 min on ice. Nuclei were isolated by centrifugation for 5 min at 760 g and resuspended in 500 μL of DpnII buffer (NEB). 15 μL of SDS 10% were added to the tube and incubated for 60min at 37°C shaking at 900rpm. Then, 150 μL of 10% Triton X-100 were added and the sample was incubated for 60 min at 37°C. Afterward, digestion of the nuclei was achieved by addition of 400U DpnII (NEB) and o/n incubation at 37°C. The next morning, 200U DpnII were added again and the sample was incubated for 4 more hours at 37°C, afterward DpnII was inactivated for 20min at 65°C. Digested nuclei were pelleted by centrifugation for 5 min at 600 g and resuspended in 5.7mL milli-Q H2O. Then, 700 μL T4 ligation buffer (Promega) and 20 μL T4 ligase (Promega, 3 U/μL) were added. The samples were incubated overnight at 16°C. The samples were then digested with 5 μL RNAse A (10 mg/μL) and 10 μL proteinase K (10 mg/mL) for 30min at 37°C and decrosslinked o/n at 65°C. DNA was purified by phenol-chloroform extraction and ethanol precipitation and quantified with the Qubit™ dsDNA HS Assay Kit (Thermo Fisher). A total of 5 μg of DNA were sonicated with a Covaris S2 instrument with the following parameters: duty cycle 10%, intensity 4, cycles per burst 200 and time 60 s. Sequencing libraries were prepared as described (Schwartzman et al., 2016). The procedure is based in a nested PCR using oligonucleotides aligned to a specific region functioning as ''bait'' or ''point of view'' for capturing contacts. The sequences of the primers used can be found in Table S1. Libraries were sequenced in an Illumina NovaSeq instrument to achieve a depth of >1 million reads per library PE 150bp. UMI-4C analysis was performed using the *UMI4Cats* R package (Ramos-Rodríguez et al., 2021). The reads were aligned on hg19 Human genome assembly. For differential testing the function *fisherUMI4C* (included in the package) was applied, performing a Fisher's Exact Test in the experiment region using a bin size of 10kb.

HiChIP

HiChIP was performed mainly as described (Mumbach et al., 2016) starting with 20 million HepG2 CTL cells. After *In situ* contact library generation, samples were sonicated in a Covaris M220 with the following settings: duty cycle 10%, PIP 75W, 100 cycles/burst, time 5′. A total of 20ug of anti-H3K4me3 antibody was used to immunoprecipitate chromatin. The experiment was replicated twice and libraries sequenced at the BGI in an Illumina HiSeq 4000 obtaining 200M paired-end 50bp reads per replicate. Sequencing data from HiChIP was analyzed using the *HiCUP* (Wingett et al., 2015) pipeline version 0.7.3. The result was transformed into a *.hic* file using *juicer-pre* software from the *juicer* (Durand et al., 2016) suite. The code with the exact parameters and specifications of the analysis pipeline are available at the following repository URLs:

https://github.com/RMalinverni/Omics_miscellanea/blob/master/HiCUP_script_and_configuration.sh
https://github.com/RMalinverni/Omics_miscellanea/blob/master/Hic.pipe.clean_by_chrom.sh
https://github.com/RMalinverni/Omics_miscellanea/blob/master/HiC_post_analysis.sh.

Use of published datasets

The ChIP-Seq profile of macroH2A1 and macroH2A2 (GEO accession GSE58175) has been previously described (Douet et al., 2017). *epic2* was used to call enriched regions (Stovner and Sætrom, 2019). In addition, we have used the following datasets available from ENCODE (ENCODE Project Consortium et al., 2013): HepG2 ChIP-Seq profile of H3K27Ac (GEO accession GSM733743), RELA (GEO GSE170794), HepG2 HiC (ENCSR194SRI). The ENCODE HiC datast was processed with Juicer (Durand et al., 2016) and loops identified with the included tool HiCCUPS. From the TCGA Pan-Cancer datasets (Weinstein et al., 2013) we used ''Batch effects normalized mRNA data'' and samples with a positive (upregulation) or negative (downregulation) score of ''RABIT transcription factor regulatory impact, HiSeqV2'' (Jiang et al., 2015).

TCGA data sets were accessed and downloaded from the UCSC Xena platform (Goldman et al., 2020). The GeneHancer database (Fishilevich et al., 2017) and the TSS positions compiled in refTSS (Abugessaisa et al., 2019) were used to identify and plot gene-enhancer functional interactions. We used the 15 chromatin states as defined by the Roadmap Epigenomics Consortium (Roadmap Epigenomics Consortium et al., 2015).

The generation and analysis of RNA-Seq data for the 32 paired samples of hepatoblastoma tumor and adjacent normal liver tissue included in the present study has been described (Carrillo-Reixach et al., 2020, GSE133039). All patients have given their informed consent and the Ethical Committee for Clinical Research of the Hospital Germans Trias I Pujol (Spain) has approved the procedures.

QUANTIFICATION AND STATISTICAL ANALYSIS

In all bar plots, the height of the bar corresponds to the mean value and the bars indicate the Standard Error. In all box plots, the box signifies the upper (75th) and lower quartiles (25th), the median is represented by a horizontal line within the box and the mean is

represented by a rhombus within the box. The upper whisker extends from the upper hinge to the largest value no further than 1.5 * IQR from the hinge (where IQR is the inter-quartile range, or distance between the first and third quartiles). The lower whisker extends from the hinge to the smallest value at most 1.5 * IQR of the hinge. Data beyond the end of the whiskers are plotted individually as ''outliers''. The statistical test and comparison used to calculate p-values, number of replicates and their nature, p-values set as significance level and the number of replicates are reported in each figure and/or figure legend. Most plots were generated using ggplot2 (Wickham, 2016). All heatmaps were generated using pheatmap (https://CRAN.R-project.org/package=pheatmap). In all hetmaps, values are scaled by row unless stated otherwise. ChIP-Seq profiles and genomic features were plotted using karyoploter (Gel and Serra, 2017).